Marine Chemistry 273 (2025) 104568

Contents lists available at ScienceDirect

Marine Chemistry

journal homepage: www.elsevier.com/locate/marchem

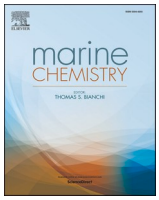

Mapping of dissolved black carbon in the Atlantic Ocean☆

Nina Davtian [a,b,*], Nuria Penalva [a], Oriol Teruel [a], Pau Comes [a], Antoni Rosell-Melé [a,1], Joan Villanueva [a]

[a] Institut de Ciència i Tecnologia Ambientals (ICTA-UAB), Universitat Autònoma de Barcelona, Bellaterra, Catalonia, Spain
[b] Aix Marseille Univ, CNRS, IRD, INRAE, CEREGE, Aix-en-Provence, France

ARTICLE INFO

Keywords:
Dissolved black carbon
Benzene polycarboxylic acids
Surface water
Water column
Atlantic Ocean

ABSTRACT

Oceanic dissolved black carbon (DBC) is the subject of a conundrum between the dominant riverine inputs in terms of mass flux and its stable and radiogenic carbon isotope composition inconsistent with a predominant riverine origin. Here, we analyzed seawater samples within specific and contrasting water masses along several latitudinal and longitudinal transects across the Atlantic Ocean to quantify DBC and map its latitudinal and water depth changes in this ocean. After comparing latitudinal changes in surface water DBC properties with those in atmospheric pyrogenic carbon inputs from seasonal, massive grass burning events in the African Savanna, we could not demonstrate the significance of atmospheric deposition as a non-riverine source of DBC in the Atlantic Ocean, likely due to the balance by DBC photo-bleaching. We found constant DBC concentrations and increasing trends in the condensation degree of DBC (i.e., B6CA:B5CA molar ratio) from surface to deep Atlantic waters and from the South Atlantic to the North Atlantic within individual shallow to deep water masses. Overall, our mapping of DBC in the Atlantic Ocean highlights the need to explore the following alternative hypotheses in the future to better understand the cycling of oceanic DBC: 1) enhanced regional atmospheric BC deposition from African savanna grassland fires impact particulate rather than dissolved BC in the Atlantic Ocean, 2) oceanic DBC has a predominantly non-pyrogenic origin, and 3) exports of terrigenous DBC across the Atlantic Ocean accompany those of terrigenous humic-like compounds from the North Atlantic via meridional circulation.

1. Introduction

Black carbon (BC) is a by-product of incomplete organic matter combustion, including natural and anthropogenic biomass burning and fossil fuel combustion, and a major component of the global carbon cycle (Goldberg, 1985; Schmidt and Noack, 2000; Mitra et al., 2013; Bird et al., 2015; Coppola et al., 2022; Vaezzadeh et al., 2023). Biomass burning is the dominant source of continental BC, mostly as post-fire residues (Kuhlbusch and Crutzen, 1995; Santín et al., 2015, 2016; Jones et al., 2019, 2020). A portion of the produced BC subsequently enters aquatic systems as particulate and dissolved BC (Jaffé et al., 2013; Bao et al., 2017; Abney and Berhe, 2018; Coppola et al., 2018; Wagner et al., 2018; Jones et al., 2020; Geng et al., 2021). The dissolved fraction represents roughly half of the BC remobilized through waterways to the oceans (Jaffé et al., 2013; Coppola et al., 2018; Jones et al., 2020).

Oceanic dissolved BC (DBC) has an estimated stock of 12–14 PgC (Dittmar and Paeng, 2009; Coppola and Druffel, 2016), which represents ~2 % of total oceanic dissolved organic carbon (DOC; estimated oceanic stock of 662 PgC; Hansell et al., 2009). Rivers are the main identified source of oceanic DBC in terms of mass flux, with an estimated flux of 27 ± 2 TgC/yr (Jaffé et al., 2013) recently reevaluated to 18 ± 4 TgC/yr (Jones et al., 2020). Photo-bleaching (estimated flux of 20–490 TgC/yr; Stubbins et al., 2012) and adsorption onto sinking particles (estimated flux from 16 to 40–85 TgC/yr; Coppola et al., 2014; Yamashita et al., 2022) are the two main identified sinks for oceanic DBC.

Oceanic DBC is presumably part of the refractory fraction of oceanic DOC (Ziolkowski and Druffel, 2010; Cai and Jiao, 2023; Coppola et al., 2024), with ^{14}C ages of 4800 ± 620 and 23,000 ± 3000 ^{14}C years for surface and deep oceanic DBC, respectively (Coppola and Druffel, 2016). However, these ^{14}C ages of oceanic DBC disagree by 1–2 orders of magnitude with an oceanic DBC age of ~700 years inferred from mass balance equations, assuming a riverine DBC flux of 18 ± 4 TgC/yr

☆ This article is part of a Special issue entitled: 'Marine black carbon' published in Marine Chemistry.

* Corresponding author at: Institut de Ciència i Tecnologia Ambientals (ICTA-UAB), Universitat Autònoma de Barcelona, Bellaterra, Catalonia, Spain.
E-mail address: davtian@cerege.fr (N. Davtian).

[1] Prof. Antoni Rosell-Melé passed away in December 2021.

https://doi.org/10.1016/j.marchem.2025.104568
Received 14 June 2024; Received in revised form 20 February 2025; Accepted 30 September 2025
Available online 1 October 2025

(Jones et al., 2020) and an oceanic DBC stock of 12–14 PgC (Dittmar and Paeng, 2009; Coppola and Druffel, 2016). Compound-specific stable carbon isotope ($\delta^{13}C$) measurements show that oceanic DBC is ~6 ‰ enriched in ^{13}C compared to riverine DBC, which reveals another inconsistency with a predominant riverine source of oceanic DBC (Wagner et al., 2019). This conundrum motivates the quest for non-riverine sources of oceanic DBC, such as atmospheric deposition (estimated flux of 2–12 TgC/yr; Jurado et al., 2008; Bao et al., 2017; Geng et al., 2021) and hydrothermal inputs (estimated flux of 1.6–9.7 TgC/yr; Dittmar and Koch, 2006; Yamashita et al., 2023).

Another challenge for the full understanding of DBC lies in the operational nature of BC definition (Qi et al., 2021; Wagner et al., 2021a), as no existing analytical method covers the full BC continuum (Hammes et al., 2007; Roth et al., 2012; Wagner et al., 2018, 2021a). The BC continuum ranges from non-aromatic, sugar-like compounds (e.g., levoglucosan; Kuo et al., 2011) to polycondensed aromatic structures (Goldberg, 1985; Ziolkowski et al., 2011; Bird et al., 2015) and consists in multiple chemical property continuums (e.g., biolability, photolability, water solubility, and atomic ratios) and a combustion continuum (Hedges et al., 2000; Masiello, 2004; Bird et al., 2015; Wagner et al., 2018; Coppola et al., 2022). For DBC analysis in oceans and other aquatic systems, the benzene polycarboxylic acid (BPCA) method is the most commonly applied approach (e.g., Dittmar and Paeng, 2009; Dittmar et al., 2012; Stubbins et al., 2012; Coppola and Druffel, 2016; Fang et al., 2017, 2018a, 2018b, 2021a, 2021b, 2021c; Nakane et al., 2017; Coppola et al., 2019, 2024Wagner et al., 2019, 2021b; Drake et al., 2020; Kelly et al., 2021; Mori et al., 2021; Yamashita et al., 2022, 2023; Bao et al., 2023; Barton et al., 2024; Speidel et al., 2024; Zhang et al., 2024a, 2024b). The BPCA method consists in oxidizing the polyaromatic BC structures into BPCAs with 3–6 carboxylic acid moieties using nitric acid (HNO_3) at high temperature and then converting individual BPCA marker concentrations into BC concentrations with a conversion factor (Glaser et al., 1998; Dittmar, 2008; Ziolkowski and Druffel, 2010; Ziolkowski et al., 2011; Stubbins et al., 2015). Despite the widespread assumption that BPCAs with 5 and 6 carboxylic acid moieties, named B5CA and B6CA, have an exclusively pyrogenic origin (Kappenberg et al., 2016), polycondensed aromatic structures of non-pyrogenic origin, such as petrogenic organic carbon and humic acids, may also yield BPCAs, including the B5CA and B6CA markers, following oxidation with HNO_3 (Hindersmann and Achten, 2017; Chang et al., 2018; Goranov et al., 2021; Yin et al., 2024).

The Atlantic Ocean constitutes an ideal test bench to assess the contribution of airborne pyrogenic BC deposition to oceanic DBC. The Atlantic Ocean not only receives substantial discharge from several major rivers (Amazon, Congo, Orinoco, Mississippi, Paraná, and St. Lawrence; Dai and Trenberth, 2002) which deliver large amounts of DBC (Dittmar et al., 2012; Coppola et al., 2019; Drake et al., 2020), but also substantial airborne inputs of pyrogenic BC from seasonal, massive grass burning events in the African Savanna (Fig. S1; Cahoon et al., 1992; Eglinton et al., 2002; Randerson et al., 2005; Pohl et al., 2014; Global Modeling and Assimilation Office GMAO, 2015; van der Werf et al., 2017; Kirago et al., 2022). Airborne BC from African savanna grassland fires also has a ^{13}C-enriched signature characteristic of C4 vegetation (Eglinton et al., 2002; Pohl et al., 2014; Kirago et al., 2022). Recent analyses of BC derived from the chemothermal oxidation method coupled to polycyclic aromatic hydrocarbon analysis in deep-sea sediments from five regions in the subtropical Atlantic Ocean support the imprint of enhanced regional atmospheric BC deposition from African savanna grassland fires on sedimentary BC, with six times higher BC accumulation rates and a ^{13}C-enriched signature in the Sierra Leone Rise compared to the Northwest Argentina Basin (St Laurent et al., 2023). An even more recent study of sedimentary BC across the equatorial Atlantic Ocean revealed an eastward ^{13}C enrichment of sedimentary BC despite constant BC fluxes (Katz et al., 2024).

While the Pacific Ocean recently benefited from multi-layer DBC analyses along several latitudinal and longitudinal transects (Fig. S1; Yamashita et al., 2022, 2023), such a DBC mapping exercise is still missing for the Atlantic Ocean (Ziolkowski and Druffel, 2010; Stubbins et al., 2012; Coppola and Druffel, 2016; Wagner et al., 2017a, 2019). All published DBC studies with Atlantic Ocean samples focus on a few sites within this ocean and collectively provide a DBC dataset mostly focused on surface waters (Fig. S1).

In this study, we analyze DBC in the water column along several latitudinal and longitudinal transects across the Atlantic Ocean. Our transects not only cover a wide range of atmospheric BC concentrations, but also a wide range of environmental conditions within the Atlantic Ocean. Our water column profiles in the Atlantic Ocean are located away from major river mouths and target specific water masses with distinct properties and sources (Figs. S1 and S2). Accordingly, our mapping of DBC in the Atlantic Ocean has two main goals: 1) assessing the imprint of enhanced regional atmospheric BC deposition from African savanna grassland fires on DBC in surface and deep waters in the Atlantic Ocean and 2) characterizing specific water masses in the Atlantic Ocean from the DBC point of view.

2. Materials and methods

2.1. Sampled water masses

The Atlantic Ocean water column comprises four main layers below the mixed layer (Liu and Tanhua, 2021). The upper layer (upper ~500–1000 m, above the neutral density isoline of 27.10 kg/m^3) consists in North Atlantic Central Water and South Atlantic Central Water (SACW; Tomczak and Godfrey, 1994; Stramma and England, 1999; Jenkins et al., 2015; Liu and Tanhua, 2021). Tomczak and Godfrey (1994) described the upper layer water mass most sampled for this study, SACW (Section 2.2), as the water mass south of 15°N with a temperature–salinity curve that connects the points 5 °C, 34.3 and 20 °C, 36.0. Liu and Tanhua (2021) reported the following conservative temperature and absolute salinity ranges for SACW: 12.30–16.30 °C and 34.294–35.936 g/kg for Western SACW with a formation area at 25–60°W, 30–45°S, and 100–1000 dbar (Stramma and England, 1999; Álvarez et al., 2014), and 9.44–13.60 °C and 34.900–35.398 g/kg for Eastern SACW with a formation area at 0–15°E, 30–40°S, and 200–700 dbar (Stramma and England, 1999). SACW predominates in the upper layer from ~50°S to ~10–15°N (Liu and Tanhua, 2021) and includes a variety of Subtropical Mode Water (also named 13 °C Water; Tsuchiya, 1986) due to Agulhas Current influences (Stramma and England, 1999). The eastern tropical Atlantic Ocean comprises an oxygen minimum zone (OMZ) from 20°S to 20°N, with hypoxic rather than anoxic conditions at 100–900 m (oxygen minimum values at 300–500 m of ~17 μmol/kg and >40 μmol/kg in the South Atlantic and North Atlantic, respectively; e.g., Stramma and England, 1999; Mercier et al., 2003; Stramma et al., 2005, 2008; Karstensen et al., 2008; Jenkins et al., 2015; Liu and Tanhua, 2021). Over the eastern tropical Atlantic Ocean OMZ, Eastern SACW in an important component, as this water mass is also found in most of the North Atlantic despite the North Atlantic Central Water predominance (Liu and Tanhua, 2021).

The intermediate layer (~1000–2000 m, between the neutral density isolines of 27.10 and 27.90 kg/m^3) comprises a nutrient content maximum (nitrate and phosphate, also silicate to a lower extent) and the lowest salinity values which characterize Antarctic Intermediate Water (AAIW; Tomczak and Godfrey, 1994; Talley, 1996; Stramma and England, 1999; Jenkins et al., 2015; Liu and Tanhua, 2021). Liu and Tanhua (2021) defined the formation area at 25–55°W, 45–60°S, and 100–300 dbar (Stramma and England, 1999; Saenko and Weaver, 2001) and reported the following averaged (mean ± standard deviation) conservative temperature, absolute salinity, and silicate, phosphate, and nitrate contents for AAIW: 1.78 ± 1.02 °C, 34.206 ± 0.083 g/kg, 21.09 ± 4.66 μmol/kg, 1.95 ± 0.11 μmol/kg, and 27.33 ± 1.92 μmol/kg. After its formation, AAIW subducts and spreads northwards within the intermediate layer where it predominates in the South Atlantic (Piola and

Gordon, 1989; Tomczak and Godfrey, 1994; Tsuchiya et al., 1994; Stramma and England, 1999; Liu and Tanhua, 2021). AAIW then reaches the equator and 30°N in increasingly diluted forms (Tsuchiya, 1989; Reid, 1994; Tomczak and Godfrey, 1994; Tsuchiya et al., 1994; Kirchner et al., 2009; Jenkins et al., 2015; Liu and Tanhua, 2021). The salinity minimum that we used to identify AAIW (Section 2.2) thus gradually weakens and AAIW temperature increases along with meridional circulation across the Atlantic Ocean (e.g., Tomczak and Godfrey, 1994; Talley, 1996; Stramma and England, 1999; Jenkins et al., 2015; Liu and Tanhua, 2021). A dissolved oxygen (DO) content maximum (300.7 ± 16.2 μmol/kg; Liu and Tanhua, 2021) also characterizes AAIW but this DO content maximum becomes weak to absent north of 15°S in the west and 25°S in the east (Reid, 1989; Stramma and England, 1999), as the eastern tropical Atlantic Ocean OMZ is located close to the boundary between SACW and AAIW and also reaches the latter (Mercier et al., 2003; Stramma et al., 2005). The intermediate layer shows higher temperature and salinity values at 25–50°N due to Mediterranean Outflow Water (MOW; Ambar and Howe, 1979; Tomczak and Godfrey, 1994; Jenkins et al., 2015; Carracedo et al., 2016; Liu and Tanhua, 2021). For MOW, Liu and Tanhua (2021) defined the formation area at 6–24°W, 33–48°N, and >300 dbar (Baringer and Price, 1997) and reported the averaged conservative temperature and absolute salinity of 12.21 ± 0.77 °C and 36.682 ± 0.081 g/kg, respectively. MOW flows out of the Strait of Gibraltar, becomes Mediterranean Water after mixing with surrounding water masses, and is slightly denser than AAIW (Reid, 1978, 1979; Price et al., 1993; Tomczak and Godfrey, 1994; Baringer and Price, 1997; Jenkins et al., 2015; Liu and Tanhua, 2021).

The deep and overflow layer (~2000–4000 m, between the neutral density isolines of 27.90 and 28.10 kg/m^3) essentially consists in North Atlantic Deep Water (NADW; Tomczak and Godfrey, 1994; Stramma and England, 1999; Jenkins et al., 2015; Liu and Tanhua, 2021). While treated as a single water mass for this study (Section 2.2), NADW is the product of several water masses formed in the North Atlantic and with contrasting properties (e.g., Liu and Tanhua, 2021). South of 40°N, Liu and Tanhua (2021) defined NADW with a redefining area at 32–50°W, 40–50°N, and 1200–3000 dbar, with a boundary at 2000 dbar between the redefining areas of upper and lower NADW (Dickson and Brown, 1994; Stramma et al., 2004). For NADW south of 40°N, Liu and Tanhua (2021) reported averaged conservative temperature, absolute salinity, and DO, silicate, phosphate, and nitrate contents of ~3.0–3.3 °C, ~35.07–35.08 g/kg, ~280 μmol/kg, ~11–13 μmol/kg, ~1 μmol/kg, and ~17 μmol/kg, respectively. NADW thus corresponds to a maximum in salinity and DO content below AAIW (e.g., Tomczak and Godfrey, 1994; Stramma and England, 1999; Jenkins et al., 2015; Liu and Tanhua, 2021), which we used to identify NADW (Section 2.2). South of 40°N, NADW spreads southwards and is present throughout the Atlantic Ocean until ~50°S (Liu and Tanhua, 2021).

The bottom layer (>4000 m, below the neutral density isoline of 28.10 kg/m^3) shows the lowest temperature values and elevated nutrient contents, especially silicate, which characterize Antarctic Bottom Water (AABW; Tomczak and Godfrey, 1994; Stramma and England, 1999; Jenkins et al., 2015; Liu and Tanhua, 2021). AABW is the product of two southern water masses formed in the Weddell Sea and with distinct properties (e.g., Foldvik and Gammelsrød, 1988; Orsi et al., 1999; Stramma and England, 1999; van Heuven et al., 2011; Álvarez et al., 2014; Liu and Tanhua, 2021). Liu and Tanhua (2021) defined the formation area at >63°S in the Weddell Sea region south of the Antarctic Circumpolar Current (Weiss et al., 1979; Orsi et al., 1999) and reported the following averaged conservative temperature, absolute salinity, and DO, silicate, phosphate, and nitrate contents for AABW: −0.46 ± 0.24 °C, 34.830 ± 0.009 g/kg, 239.0 ± 9.3 μmol/kg, 124.87 ± 2.36 μmol/kg, 2.27 ± 0.03 μmol/kg, and 32.82 ± 0.45 μmol/kg. After leaving its formation area, AABW sinks to the bottom and spreads northwards across the South Atlantic, including the Argentine Basin, then the Brazil Basin after passing through the Vema Channel, where AABW essentially disappears at 4.5°S following water exchange with NADW between 50°S and the equator (Siedler et al., 1996; Stramma and England, 1999; van Heuven et al., 2011; Liu and Tanhua, 2021). We identified AABW in three South Atlantic water column profiles that show bottom waters at >5000 m and <1 °C (Section 2.2).

The South Atlantic Ocean also comprises southern water masses other than AAIW and AABW, Upper Circumpolar Deep Water (UCDW) and Lower Circumpolar Deep Water, which are colder, fresher, oxygen-poor, and nutrient-rich compared with NADW (Reid, 1989; Tsuchiya et al., 1994; Stramma and England, 1999; Liu and Tanhua, 2021). For Lower Circumpolar Deep Water, Liu and Tanhua (2021) defined the formation area at <60°W, 55–65°S, and 200–1000 dbar and reported the following averaged conservative temperature, absolute salinity, and DO, silicate, phosphate, and nitrate contents: 0.41 ± 0.19 °C, 34.850 ± 0.011 g/kg, 203.8 ± 8.5 μmol/kg, 115.53 ± 7.72 μmol/kg, 2.31 ± 0.06 μmol/kg, and 33.46 ± 0.91 μmol/kg. Circumpolar Deep Water is formed from the large-scale mixing of several water masses in the Antarctic Circumpolar Current region, including NADW that is itself deflected upwards by AABW at ~50°S before reaching the Antarctic Circumpolar Current (van Heuven et al., 2011; Liu and Tanhua, 2021). After its formation, Circumpolar Deep Water flows eastward in the Antarctic Circumpolar Current before splitting into two branches at ~60°S (Reid, 1989; Tsuchiya et al., 1994; Stramma and England, 1999; Liu and Tanhua, 2021). The upper branch, UCDW, is upwelled and partly joins the AAIW before spreading northwards in the South Atlantic to ~22°S at 25°W, including the Argentine Basin, whereas the rest of UDCW spreads towards the coastal region, mixes with the cold fresh shelf water, sinks to the bottom and contributes to AABW along with Lower Circumpolar Deep Water (Tsuchiya et al., 1994; Stramma and England, 1999; Marshall and Speer, 2012; Abernathey et al., 2016; Liu and Tanhua, 2021). North of ~22°S at 25°W, the eastern tropical Atlantic Ocean OMZ obscures the UCDW signature, which we identified with the oxygen minimum between AAIW and NADW in the South Atlantic (Section 2.2; Tsuchiya et al., 1994; Stramma and England, 1999).

2.2. Field sampling and DOC extraction

Seawater sampling was conducted in the Atlantic Ocean during the R/V Sarmiento de Gamboa SAGA10W cruise (SAGA10) in March–April 2021 and during the R/V Hesperides PYROWIND cruise (PYRO22) in April–May 2022 (Fig. 1). Within the South Atlantic Ocean (SAGA10), 12 seawater samples were collected in 3 water column stations from both Atlantic (mixed layer, SACW, and NADW) and Antarctic water masses (AAIW, UCDW, and AABW). Within the tropical Atlantic Ocean (PYRO22), 48 seawater samples were collected in 12 water column stations from Atlantic (deep chlorophyll maximum, OMZ, and NADW), Antarctic (AAIW and AABW), and Mediterranean water masses (MOW). Water column samples were collected using Niskin bottles. Pressure, temperature, conductivity, salinity, DO content, and fluorescence were measured with a conductivity-temperature-depth sensor (see Fig. S2 and Table S1 for the results at the sampling depths). Only the SAGA10 cruise benefited from a post-cruise calibration of the DO sensor with the Winker titration method, which was not applied for this study for the sake of consistent data processing for both SAGA10 and PYRO22 cruises. The apparent oxygen utilization (AOU) was calculated as the difference between the saturated and measured DO concentrations (see Fig. S2 and Table S1 for the results at the sampling depths; saturated DO concentrations calculated following Weiss, 1970). During transit periods, 12 surface water samples (~5 m water depth) were collected along a latitudinal transect using an underway pumping system. The measured temperature and salinity of sampled sea surface waters are reported in Fig. S3 and Table S1.

Between 18 and 50 L of seawater were processed for DOC extraction following the solid phase extraction (SPE) method by Dittmar et al. (2008). The seawater was filtered using a muffled (450 °C overnight) glass fiber (SAGA10) or quartz filter (PYRO22) of a 0.7 μm nominal pore size (Whatman). Immediately after sampling, the seawater filtrate was

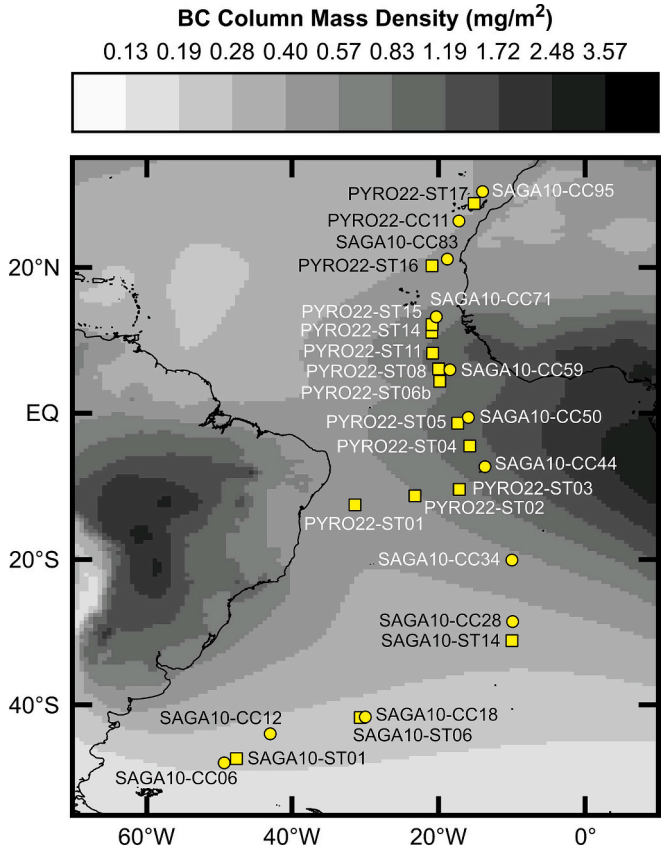

Fig. 1. Seawater sample locations. Squares, water column stations; circles, surface water samples; and background, time-averaged atmospheric black carbon column mass density (MERRA-2 NASA atmospheric reanalysis, M2TMNXAER v5.12.4) from 1980 to 2022 (https://giovanni.gsfc.nasa.gov/giovanni/;https://giovanni.gsfc.nasa.gov/giovanni/; Acker and Leptoukh, 2007; Global Modeling and Assimilation Office GMAO, 2015; Buchard et al., 2017; Gelaro et al., 2017; Randles et al., 2017).

acidified to a pH of 2 with concentrated HCl. The DOC was extracted from the acidified filtrate using an SPE cartridge (5 g, 40 mL, Bond Elut PPL, Agilent) following Dittmar et al. (2008). The SPE-DOC extracts in MeOH were stored at −20 °C in the dark until further processing. The expected recovery of SPE-DOC is 40–52 % of total DOC in marine waters (Dittmar et al., 2008; Wagner et al., 2019).

2.3. SPE-DOC quantification and isotopic characterization

The SPE-DOC extracts were dried at 50 °C under a N_2 flow using a TurboVap (Biotage). The SPE-DOC samples were then redissolved in MeOH for further processing. To quantify SPE-DOC and determine its $\delta^{13}C$ values, aliquots of SPE-DOC samples were placed in tin capsules. The MeOH was evaporated to dryness with an oven set to 50 °C. The tin capsules were then folded and combusted using a Thermo Flash EA Isolink CN coupled to a Thermo Delta V Advantage IRMS for SPE-DOC quantification and $\delta^{13}C$ analysis. The standard deviation of replicate EA-IRMS reference material measurements was better than 0.1 ‰. Capsule and MeOH blanks were run with every batch of EA-IRMS analyses for quality control and yielded negligible amounts of carbon compared with SPE-DOC samples.

2.4. DBC quantification

DBC analysis follows the BPCA protocol by Penalva-Arias et al. (2024) with simplifications related to the different sample matrix. Aliquots of SPE-DOC samples were placed in 55 mL MARSXpress (CEM Corp.) vessels. The MeOH was evaporated to dryness using a MARS6 XpressVap evaporation system (CEM Corp.) during 3–5 min before SPE-DOC oxidation with 5 mL of 67–69 % HNO_3 (trace metal grade, Fisher Scientific, Leicestershire, UK) for 6 h at 160 °C in a MARS 6 microwave (CEM Corp.). The samples were heated to 160 °C in 10 min and then this temperature was held for 6 h. After sample oxidation, the HNO_3 was evaporated to dryness using the MARS6 XpressVap evaporation system during 25 min. The oxidized extracts were transferred with MeOH into glass injection vials and vacuum-dried at 40 °C. Samples were redissolved in 0.5 mL of 2 % phosphoric acid (Sigma-Aldrich) in ultrapure water (LC phase A) and filtered with a 0.45 μm PTFE filter prior to LC-UV analysis.

BPCAs were analyzed using a high-performance liquid chromatography system consisting of a quaternary pump (Agilent 1290 Infinity), an automatic sample injector (Agilent 1290 Infinity), and a diode array detector (Agilent 1260 Infinity). The LC column used was an Agilent Poroshell 120 SB-C18 column (3 × 100 mm, 2.7 μm) thermostated at 25 °C and with a mobile phase flow rate of 0.5 mL/min. Compounds were eluted using a solvent gradient from 100 % A to 30 % A in 10 min followed by isocratic conditions during 2 min. The column was conditioned during 7 min with 100 % A between each sample analysis. Solvent A was obtained by diluting 1.1 mL of 85 % phosphoric acid with 0.5 L of ultrapure water. Solvent B was acetonitrile (HPLC-grade, Merck). BPCAs were detected and quantified by their absorbance at 240 nm (see Fig. S4 for examples of LC-UV chromatograms). BPCA detection and quantification was performed by comparing their absorbance at 240 nm with standard solutions using an external linear calibration curve. The dynamic range is of 0.5 to 100 μg/mL for B6CA and B5CA. The linear calibration curve was adjusted using the minimum squared regression method, weighted by the inverse of the squared concentration ($1/x^2$; Gu et al., 2014). Instrumental control and data acquisition were performed with the MassHunter Workstation software version 10.0 SR1 (Agilent). Peak integration, instrumental calibration, and quantification were performed with the Quantitative Analysis Module of the MassHunter Workstation version 10.1 (Agilent). Sample DBC concentrations were calculated using the established power relationship between DBC (μM-C) and the sum of B6CA and B5CA (nM-BPCA) by Stubbins et al. (2015): $[DBC] = 0.0891 \times ([B6CA + B5CA])^{0.9175}$ ($n = 352$, $R = 0.998$, $p < 0.0001$).

One SPE-DOC sample was selected to assess the method repeatability. The replicate analyses ($n = 5$) yielded relative standard deviations better than 10 % for B6CA and B5CA concentrations and a standard deviation of ±0.01 for B6CA:B5CA molar ratios. One or two procedural blanks were run with every batch of samples for quality control and all yielded negligible amounts of BPCAs compared with SPE-DOC samples.

2.5. Statistical analyses and data mapping

Statistical analyses for this study were conducted using the R software (version 4.4.2; R Core Team, 2024). Means were compared without the assumption of equal variances with Welch's one-way analyses of variance (ANOVA) tests (Welch, 1951) using the "oneway.test" R function. In case of significant differences in means based on the Welch's one-way ANOVA tests ($p < 0.05$), paired comparisons of means were carried out with Games-Howell post-hoc tests (Howell, 2010) using the "games_howell_test" function from the "rstatix" R package (Kassambara, 2023). Principal component analysis (PCA) and handling of missing data in multivariate analysis were carried out using the "FactoMineR" (Lê et al., 2008) and "missMDA" (Josse and Husson, 2016) R packages, respectively. Pearson correlation tests and ordinary least squares regression analyses were carried out using the "cor.test" and "lm" R functions, respectively, with $p < 0.05$ as the cut-off for significance.

Maps were created using the QGIS (version 3.34.4 LTR, https://qgis.org/) and Ocean Data View (version 5.7.2, https://odv.awi.de/; Schlitzer, 2024) softwares. Atmospheric BC column mass density (MERRA-2

version 5.12.4 https://doi.org/10.5067/FH9A0MLJPC7N, accessed 11 August 2023; Global Modeling and Assimilation Office GMAO, 2015; Buchard et al., 2017; Gelaro et al., 2017; Randles et al., 2017) and surface water absorption due to chromophoric dissolved organic matter (CDOM) and detrital material at 443 nm ($a_{CDOM}(443)$; SeaWiFS version R2022.0 https://doi.org/10.5067/ORBVIEW-2/SeaWiFS/L3M/IOP/2022.0, accessed 18 December 2024; Garver and Siegel, 1997; Maritorena et al., 2002; NASA Goddard Space Flight Center, Ocean Ecology

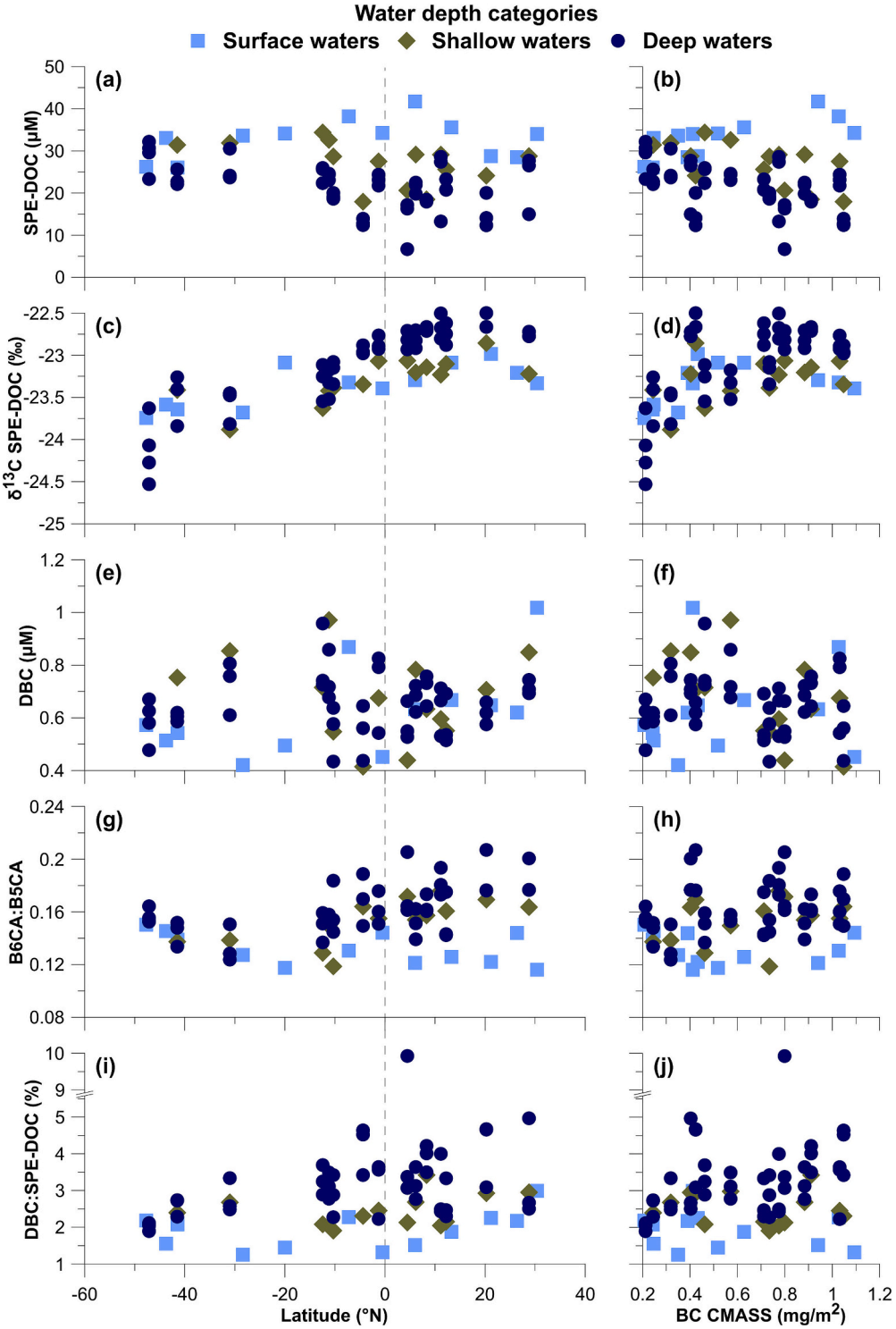

Fig. 2. Changes in SPE-DOC and DBC properties in the Atlantic Ocean with latitude (left) and atmospheric BC inputs from Africa (right). (a) and (b) SPE-DOC concentration, (c) and (d) SPE-DOC $\delta^{13}C$ composition, (e) and (f) DBC concentration, (g) and (h) B6CA:B5CA molar ratio, and (i) and (j) DBC molar proportion in SPE-DOC. Water depth categories consist in: surface waters, underway samples; shallow waters, water column samples from the mixed layer and deep chlorophyll maximum; and deep waters, water column samples deeper than the mixed layer and deep chlorophyll maximum. Atmospheric BC inputs are inferred using time-averaged atmospheric black carbon column mass density (MERRA-2 NASA atmospheric reanalysis, M2TMNXAER v5.12.4) from 1980 to 2022 (https://giovanni.gsfc.nasa.gov/giovanni/; Acker and Leptoukh, 2007; Global Modeling and Assimilation Office GMAO, 2015; Buchard et al., 2017; Gelaro et al., 2017; Randles et al., 2017).

Laboratory, Ocean Biology Processing Group, 2022) data were retrieved from the Giovanni website (https://giovanni.gsfc.nasa.gov/giovanni/; Acker and Leptoukh, 2007). Time averages for this study were determined from 1980 to 2022 (full MERRA-2 timespan until the year of the PYRO22 cruise) and from 1997 to 2010 (full SeaWiFS timespan) for atmospheric BC column mass density and $a_{CDOM}(443)$, respectively.

3. Results

3.1. SPE-DOC concentration

A division of the dataset into surface water samples (n = 12; underway samples taken at ~5 m water depth), shallow water samples (n = 14; mixed layer and deep chlorophyll maximum samples), and deep-water samples (n = 46; other water column samples) offered an initial characterization of SPE-DOC and DBC in the Atlantic Ocean. Overall, SPE-DOC concentrations ranged from 6.7 to 41.7 μM (Fig. 2a; Table S1). All three water depth groups showed statistically different averaged SPE-DOC concentrations ($F(2, 24.414) = 26.536$, $p < 0.001$; Table 1). Most water column stations showed a decrease in SPE-DOC concentrations within the first 1000 m and relatively stable SPE-DOC concentrations in deeper waters (Figs. 3b and S5). In surface waters, SPE-DOC concentration showed a significant correlation with atmospheric BC column mass density ($n = 12$, $r = 0.741$, $p < 0.006$; Fig. 2b), but not with $a_{CDOM}(443)$ ($n = 12$, $r = -0.336$, $p = 0.286$). In shallow and deep waters, SPE-DOC concentration showed a significant anti-correlation with atmospheric BC column mass density (n = 60, r = −0.445, $p < 0.001$; Fig. 2b).

3.2. SPE-DOC $\delta^{13}C$ composition

Overall, SPE-DOC $\delta^{13}C$ values ranged from −24.53 to −22.50 ‰ (Fig. 2c; Table S1). Surface waters showed statistically lighter averaged SPE-DOC $\delta^{13}C$ values compared with deep waters ($F(2, 31.172) = 3.982$, $p < 0.03$; Table 1). Most water column stations showed SPE-DOC $\delta^{13}C$ values heavier by ~0.5 ‰ in deep waters compared with shallow waters (Figs. 3c and S5), the main exceptions being the two southernmost water column stations (SAGA10 ST01 and SAGA10 ST06) and the bottom water samples (AABW) at PYRO22 ST01 and PYRO22 ST02. Overall, SPE-DOC $\delta^{13}C$ showed a significant correlation with atmospheric BC

Table 1
Averaged SPE-DOC and DBC properties (mean ± SD) for selected water masses and water depth categories. Conc., concentration; DCM, deep chlorophyll maximum; OMZ, oxygen minimum zone; AAIW, Antarctic Intermediate Water; and NADW, North Atlantic Deep Water.

		SPE-DOC		DBC		
	n	Conc. (μM)	$\delta^{13}C$ (‰)	Conc. (μM)	B6CA:B5CA	DBC:SPE-DOC (%)
Surface waters[a]	12	32.8 ± 4.7	−23.4 ± 0.3	0.62 ± 0.17	0.13 ± 0.01	1.9 ± 0.5
Shallow waters[b]	14	27.2 ± 5.2	−23.3 ± 0.3	0.68 ± 0.16	0.15 ± 0.02	2.5 ± 0.4
Deep waters[c]	46	21.4 ± 5.6	−23.1 ± 0.5	0.65 ± 0.11	0.16 ± 0.02	3.3 ± 1.3
DCM	12	26.4 ± 5.2	−23.2 ± 0.2	0.66 ± 0.16	0.16 ± 0.02	2.5 ± 0.5
OMZ	9	20.6 ± 4.8	−22.8 ± 0.2	0.61 ± 0.07	0.16 ± 0.02	3.1 ± 0.8
AAIW	15	20.7 ± 5.5	−23.0 ± 0.5	0.64 ± 0.10	0.16 ± 0.02	3.2 ± 0.7
NADW	15	21.2 ± 6.1	−23.1 ± 0.4	0.68 ± 0.12	0.17 ± 0.02	3.6 ± 1.9

[a] Underway samples.
[b] Water column samples from the mixed layer and DCM.
[c] Water column samples from all water masses deeper than the mixed layer and DCM.

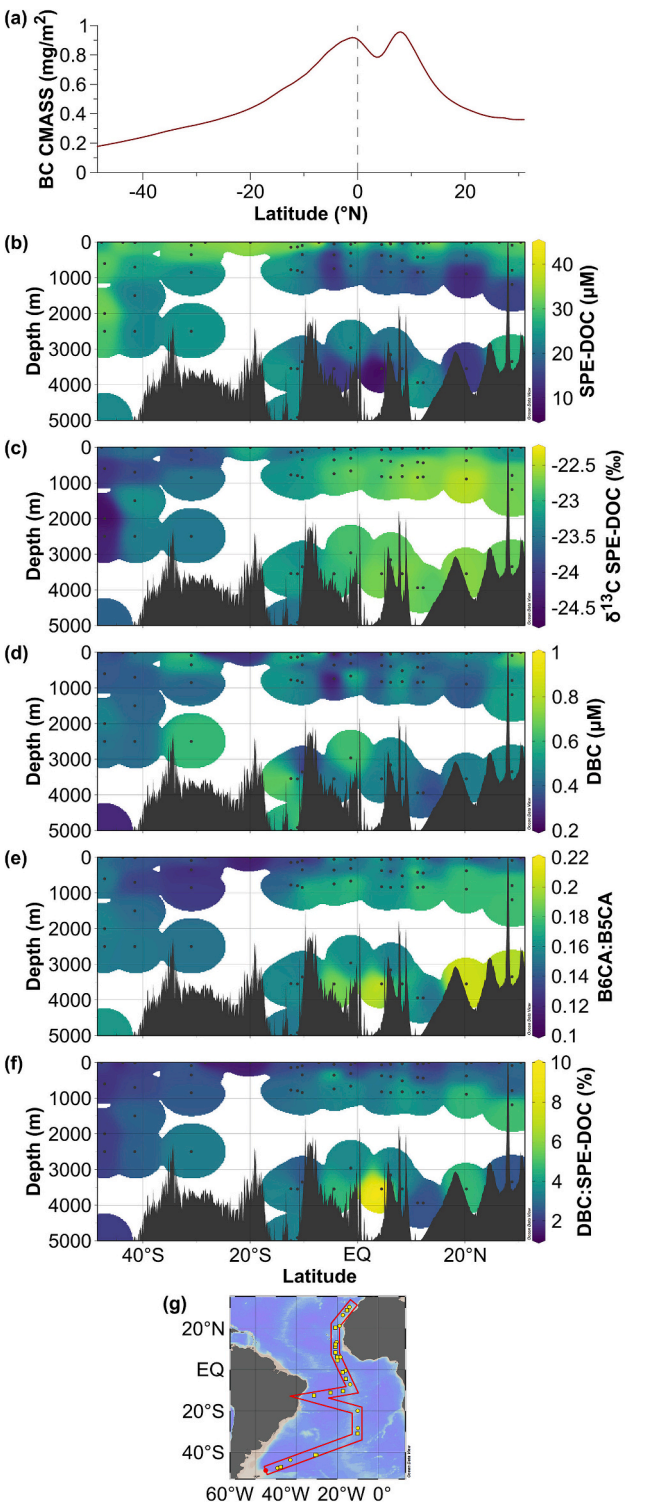

Fig. 3. Mapping of SPE-DOC and DBC properties in the Atlantic Ocean in comparison with atmospheric BC inputs from Africa. (a) Time-averaged atmospheric black carbon column mass density (MERRA-2 NASA atmospheric reanalysis, M2TMNXAER v5.12.4) from 1980 to 2022 at 20°W (https://giovanni.gsfc.nasa.gov/giovanni/; Acker and Leptoukh, 2007; Global Modeling and Assimilation Office GMAO, 2015; Buchard et al., 2017; Gelaro et al., 2017; Randles et al., 2017), (b) and (c) SPE-DOC concentration and $\delta^{13}C$ composition, (d), (e), and (f) DBC concentration, degree of condensation (B6CA:B5CA molar ratio), and molar proportion in SPE-DOC, and (g) Atlantic Ocean section as defined in Ocean Data View (Schlitzer, 2024).

column mass density ($n = 72$, $r = 0.540$, $p < 0.001$), but not when restricting to surface waters ($n = 12$, $r = 0.364$, $p = 0.245$; Fig. 2d). In surface waters, SPE-DOC $\delta^{13}C$ did not show a significant correlation with $a_{CDOM}(443)$ ($n = 12$, $r = 0.407$, $p = 0.190$).

3.3. DBC concentration and condensation degree

Overall, DBC concentrations ranged from 0.41 to 1.02 μM (Fig. 2e; Table S1). All three water depth groups showed statistically similar averaged DBC concentrations ($F(2, 19.338) = 0.362$, $p = 0.701$; Table 1). Water column stations showed inconsistent changes in DBC concentrations with water depth (Figs. 3d and S5). Overall, DBC concentration did not show a significant correlation with atmospheric BC column mass density ($n = 72$, $r = -0.109$, $p = 0.361$), including when restricting to surface waters ($n = 12$, $r = 0.158$, $p = 0.623$; Fig. 2f). In surface waters, DBC concentration did not show a significant correlation with $a_{CDOM}(443)$ ($n = 12$, $r = -0.003$, $p = 0.992$).

Overall, B6CA:B5CA molar ratios ranged from 0.12 to 0.21 (Fig. 2g; Table S1). Surface waters showed statistically lower averaged B6CA:B5CA molar ratios compared with shallow and deep waters ($F(2, 27.188) = 22.102$, $p < 0.001$; Table 1). Some water column stations (e.g., PYRO22 ST16 and PYRO22 ST17) show subtle increases in B6CA:B5CA molar ratios with water depth (Figs. 3e and S5). Overall, B6CA:B5CA molar ratio did not show a significant correlation with atmospheric BC column mass density ($n = 72$, $r = 0.206$, $p = 0.083$), including when restricting to surface waters ($n = 12$, $r = -0.201$, $p = 0.531$; Fig. 2h). In surface waters, B6CA:B5CA molar ratio did not show a significant correlation with $a_{CDOM}(443)$ ($n = 12$, $r = -0.002$, $p = 0.996$).

Overall, DBC:SPE-DOC molar ratios ranged from 1.3 to 9.9 % (Fig. 2i; Table S1). All three water depth groups showed statistically different averaged DBC:SPE-DOC molar ratios ($F(2, 34.615) = 16.458$, $p < 0.001$; Table 1). Most water column stations show subtle increases in DBC:SPE-

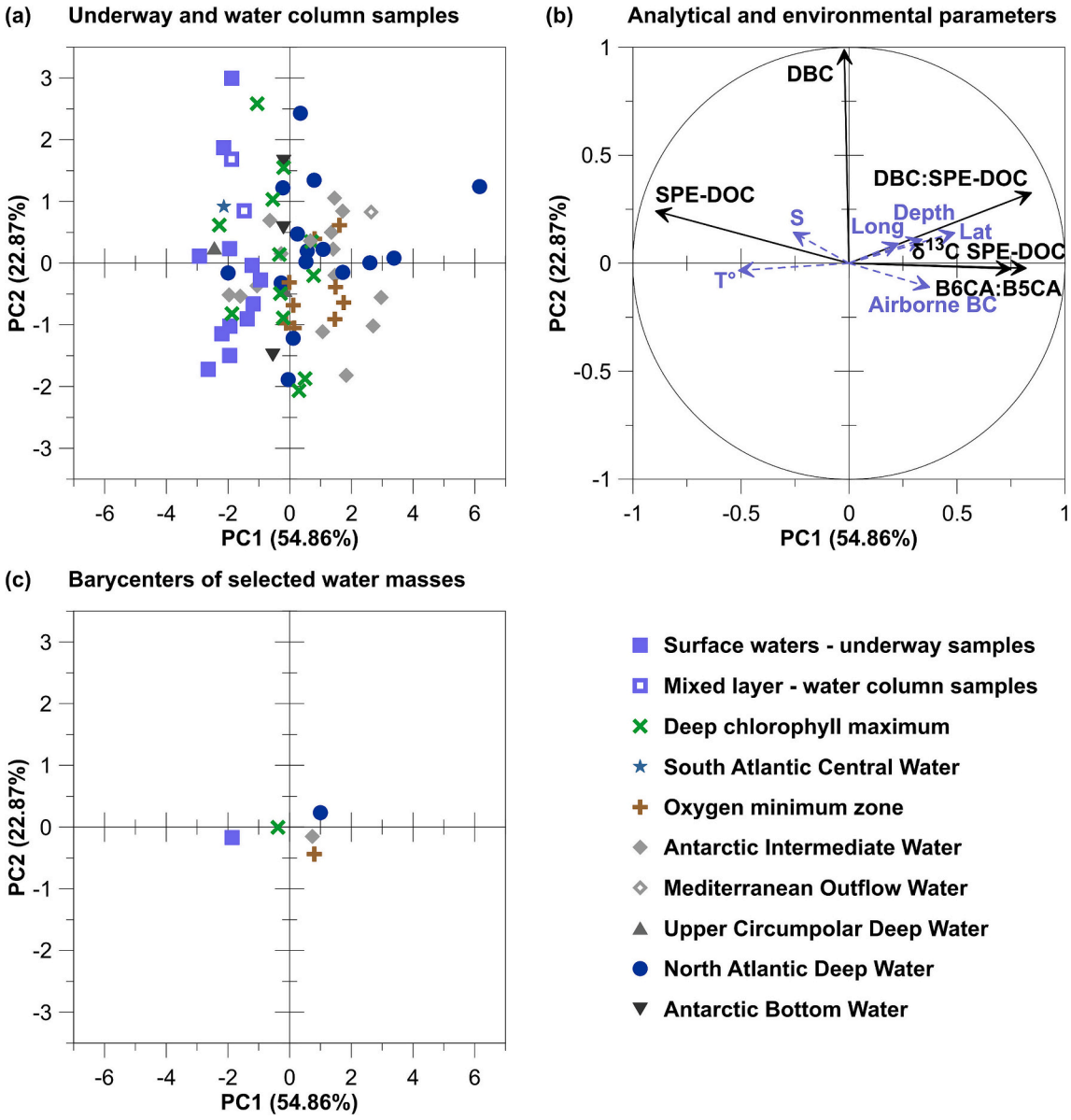

Fig. 4. Water mass characterization in the Atlantic Ocean from the SPE-DOC and DBC perspective with principal component analysis. (a) Individual surface and deep seawater samples and corresponding water masses, (b) geochemical properties as contributing variables (black solid arrows) and environmental conditions as supplementary variables (blue dashed arrows), and (c) barycenters of selected water masses. Coordinates in panel 4b correspond to *r* values for correlations between variables and principal components. Lat, latitude; Long, longitude; Airborne BC, atmospheric BC inputs; T°, temperature; and S, salinity. (For interpretation of the references to colour in this figure legend, the reader is referred to the web version of this article.)

DOC molar ratios with water depth, typically anti-correlated with decreases in SPE-DOC concentrations with water depth (Figs. 3f and S5). Overall, DBC:SPE-DOC molar ratio did not show a significant correlation with atmospheric BC column mass density ($n = 72$, $r = 0.217$, $p = 0.067$), including when restricting to surface waters ($n = 12$, $r = -0.242$, $p = 0.448$; Fig. 2j). In surface waters, DBC:SPE-DOC molar ratio did not show a significant correlation with $a_{CDOM}(443)$ ($n = 12$, $r = 0.193$, $p = 0.549$).

3.4. SPE-DOC and DBC characterization from a multivariate analysis

A PCA on the measured geochemical properties (SPE-DOC concentration and $\delta^{13}C$ composition, DBC concentration, and B6CA:B5CA and DBC:SPE-DOC molar ratios) for all seawater samples offered further characterization of SPE-DOC and DBC in the Atlantic Ocean. The first two principal components PC1 and PC2 captured 54.9 % and 22.9 % of the total variability, respectively (Fig. 4; see Figs. S6 and S7 for PCA results with only surface water samples and only water column samples, respectively). All measured geochemical variables had coordinates corresponding to strong relationships with PC1 (absolute r values >0.75; r values equivalent to coordinates of variables within the ordination space) and weak to absent relationships with PC2 ($-0.03 < r < 0.33$), except DBC concentration which had coordinates corresponding to an almost absent relationship with PC1 and an almost perfect relationship with PC2 (Fig. 4b).

Within the most sampled water masses, namely surface waters ($n = 12$), deep chlorophyll maximum ($n = 12$), OMZ ($n = 9$), AAIW ($n = 15$), and NADW ($n = 15$), seawater samples showed strong variabilities in PC2 coordinates (Fig. 4a). By contrast, the most sampled water masses followed clearer trends with water depth along the PC1 axis. The projection of latitude, longitude, and environmental variables (atmospheric BC column mass density, water depth, temperature, salinity, DO content, and fluorescence) on the first ordination plane (PC1 and PC2) showed typically poor relationships between those supplementary variables and measured geochemical variables (Figs. 4b and S7b).

When focusing on the barycenters of the most sampled water masses (surface waters, deep chlorophyll maximum, OMZ, AAIW, and NADW), PC1 distinguished three groups with different SPE-DOC concentrations and $\delta^{13}C$ values and different B6CA:B5CA and DBC:SPE-DOC molar ratios: surface waters, deep chlorophyll maximum, and OMZ–AAIW–NADW (Fig. 4c). By contrast, PC2 hardly distinguished the most sampled water masses each other, given the large variability in DBC concentrations within these water masses.

3.5. Latitudinal trends in SPE-DOC and DBC properties

Based on the regression analyses on the full dataset and restricted to each of the most sampled water masses (surface waters, deep chlorophyll maximum, OMZ, AAIW, and NADW), SPE-DOC $\delta^{13}C$ systematically showed significant latitudinal trends towards heavier values from 47.7°S to 30.4°N ($0.469 \leq R^2 \leq 0.875$, $p \leq 0.014$; Fig. 5). By contrast, DBC concentration showed no significant latitudinal trend ($0.006 \leq R^2 \leq 0.316$, $p \geq 0.057$; Fig. 5). With the exceptions of the full dataset and AAIW, SPE-DOC concentration and DBC:SPE-DOC molar ratio showed non-significant latitudinal trends ($0.039 \leq R^2 \leq 0.170$, $p \geq 0.182$; Fig. 5). Overall, SPE-DOC concentration and DBC:SPE-DOC molar ratio showed a subtle decrease ($n = 72$, $R^2 = 0.061$, $p < 0.037$) and increase ($n = 72$, $R^2 = 0.084$, $p < 0.014$), respectively, from 47.7°S to 30.4°N. In AAIW, SPE-DOC concentration and DBC:SPE-DOC molar ratio showed a modest decrease ($n = 15$, $R^2 = 0.318$, $p < 0.029$) and increase ($n = 15$, $R^2 = 0.502$, $p < 0.003$), respectively, from 47.1°S to 28.8°N. With the exceptions of surface waters and OMZ ($0.248 \leq R^2 \leq 0.282$, $p \geq 0.099$), B6CA:B5CA molar ratio showed significant latitudinal trends (Fig. 5). Overall, B6CA:B5CA molar ratio showed a subtle increase ($n = 72$, $R^2 = 0.131$, $p < 0.002$) from 47.7°S to 30.4°N. In the deep chlorophyll maximum, AAIW, and NADW, B6CA:B5CA molar ratio showed modest increases ($0.331 \leq R^2 \leq 0.509$, $p \leq 0.025$) from 47.1°S to 28.8°N.

3.6. Relationships between SPE-DOC and DBC properties and AOU–DO content

Regression analyses on the full water column dataset and restricted to each of the most sampled water masses (deep chlorophyll maximum, OMZ, AAIW, and NADW) versus AOU (Fig. 6) and DO content (Fig. S8) were carried out to complement the regression analyses of the latitudinal trends described above (Section 3.5). Overall, SPE-DOC concentration and $\delta^{13}C$ composition showed significant but subtle relationships with AOU ($n = 56$ due to missing DO data, $R^2 = 0.191$, $p < 0.001$; Fig. 6). By contrast, none of the measured DBC properties (DBC concentration and B6CA:B5CA and DBC:SPE-DOC molar ratios) showed a general significant relationship with AOU ($n = 56$ due to missing DO data, $0.024 \leq R^2 \leq 0.067$, $p \geq 0.055$; Fig. 6). In the deep chlorophyll maximum, none of the measured SPE-DOC and DBC properties showed a significant relationship with AOU ($n = 12$, $0.047 \leq R^2 \leq 0.154$, $p \geq 0.206$; Fig. 6). In the OMZ, only DBC concentration showed a significant but moderate relationship with AOU ($n = 9$, $R^2 = 0.558$, $p < 0.021$) whereas the other measured geochemical properties showed non-significant relationships with AOU ($n = 9$, $0.010 \leq R^2 \leq 0.443$, $p \geq 0.050$; Fig. 6). In AAIW, only DBC concentration showed a non-significant relationship with AOU ($n = 15$, $R^2 = 0.022$, $p = 0.597$) whereas the other measured geochemical properties showed significant and moderate to strong relationships with AOU ($n = 15$, $0.419 \leq R^2 \leq 0.783$, $p \leq 0.009$; Fig. 6). In NADW, only SPE-DOC $\delta^{13}C$ showed a significant but moderate relationship with AOU ($n = 12$ due to missing DO data, $R^2 = 0.678$, $p < 0.001$) whereas the other measured geochemical properties showed non-significant relationships with AOU ($n = 12$ due to missing DO data, $0.045 \leq R^2 \leq 0.170$, $p \geq 0.183$; Fig. 6). Our regression analyses versus DO content rather than AOU typically preserved the non-significant relationships and yielded significant trends in opposite directions, the only exceptions being the general relationship between SPE-DOC concentration and DO content which was non-significant ($n = 56$ due to missing DO data, $R^2 = 0.049$, $p = 0.099$), as well as the OMZ which showed a non-significant relationship between DBC and DO content ($n = 9$, $R^2 = 0.379$, $p = 0.078$) and a significant but moderate relationship between SPE-DOC $\delta^{13}C$ and DO content ($n = 9$, $R^2 = 0.645$, $p < 0.009$; Fig. S8).

4. Discussion

4.1. Spatial distribution and source of SPE-DOC in Atlantic waters

Overall, SPE-DOC concentrations (7 to 42 μM) are generally lower than reported concentrations for bulk-DOC (40 to 80 μM; Hansell et al., 2009; Wagner et al., 2019). The reason for this systematic difference is the relatively low recovery of SPE-DOC in marine waters (Dittmar et al., 2008; Wagner et al., 2019). Assuming a 43 % recovery of SPE-DOC (Dittmar et al., 2008), our estimates in bulk-DOC concentrations (16 to 97 μM) would mostly fall within published bulk-DOC concentrations for the Atlantic Ocean (Hansell et al., 2009; Wagner et al., 2019). However, the spatial traits of the SPE-DOC dataset reproduce the same general features as the ones previously reported using the bulk-DOC approach. For example, SPE-DOC concentration profiles mostly show maxima in surficial waters and minima at depth >1000 m, like bulk-DOC concentration profiles in open oceans (Carlson and Ducklow, 1995; Hansell and Carlson, 2001; Dittmar and Stubbins, 2014; Wagner et al., 2019). These consistent trends with water depth suggest that both bulk-DOC and SPE-DOC consist in several and diversely refractory pools (Lancelot et al., 1993; Hansell et al., 2012; Hansell, 2013; Dittmar and Stubbins, 2014; Moran et al., 2016). “SPE” and “bulk” estimates also provide similar latitudinal trends in surface waters. The tropical Atlantic Ocean tends to show higher surface water SPE-DOC concentrations (up to 42 μM) than do higher latitude regions (minimum of 26 μM; Fig. 5).

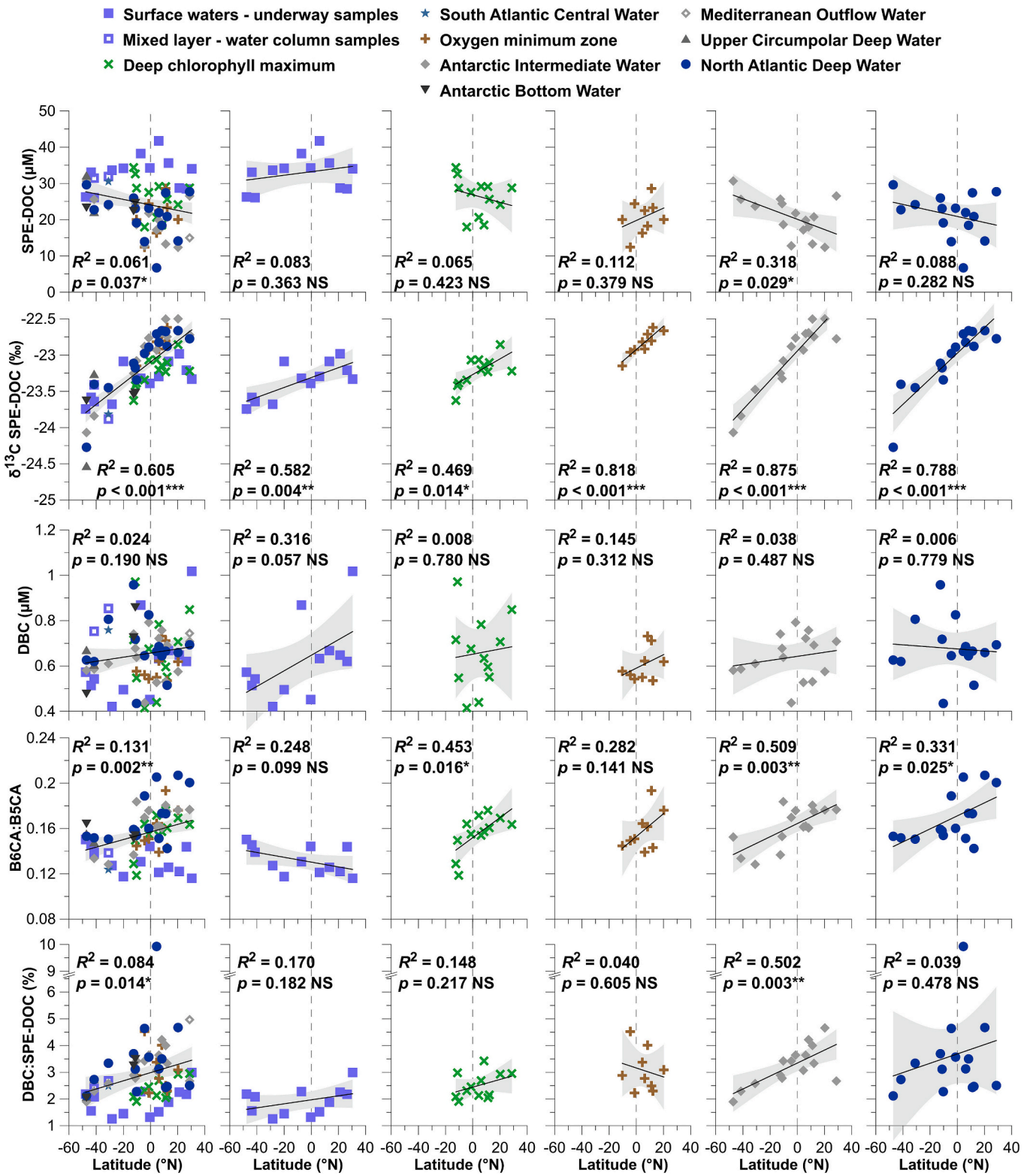

Fig. 5. Latitudinal trends in surface and deep seawater SPE-DOC and DBC properties in the Atlantic Ocean. From left to right, all seawater samples, surface waters, deep chlorophyll maximum, oxygen minimum zone, Antarctic Intermediate Water, and North Atlantic Deep Water. From top to bottom, SPE-DOC concentration and $\delta^{13}C$ composition and DBC concentration, degree of condensation (B6CA:B5CA molar ratio), and molar proportion in SPE-DOC. Grey shadings indicate the 95 % confidence intervals of the linear regressions. Determination R^2 coefficients and p-values for each linear regression are also shown, with their significance levels coded as follows: NS, not significant; *, $p < 0.05$; **, $p < 0.01$; and ***, $p < 0.001$.

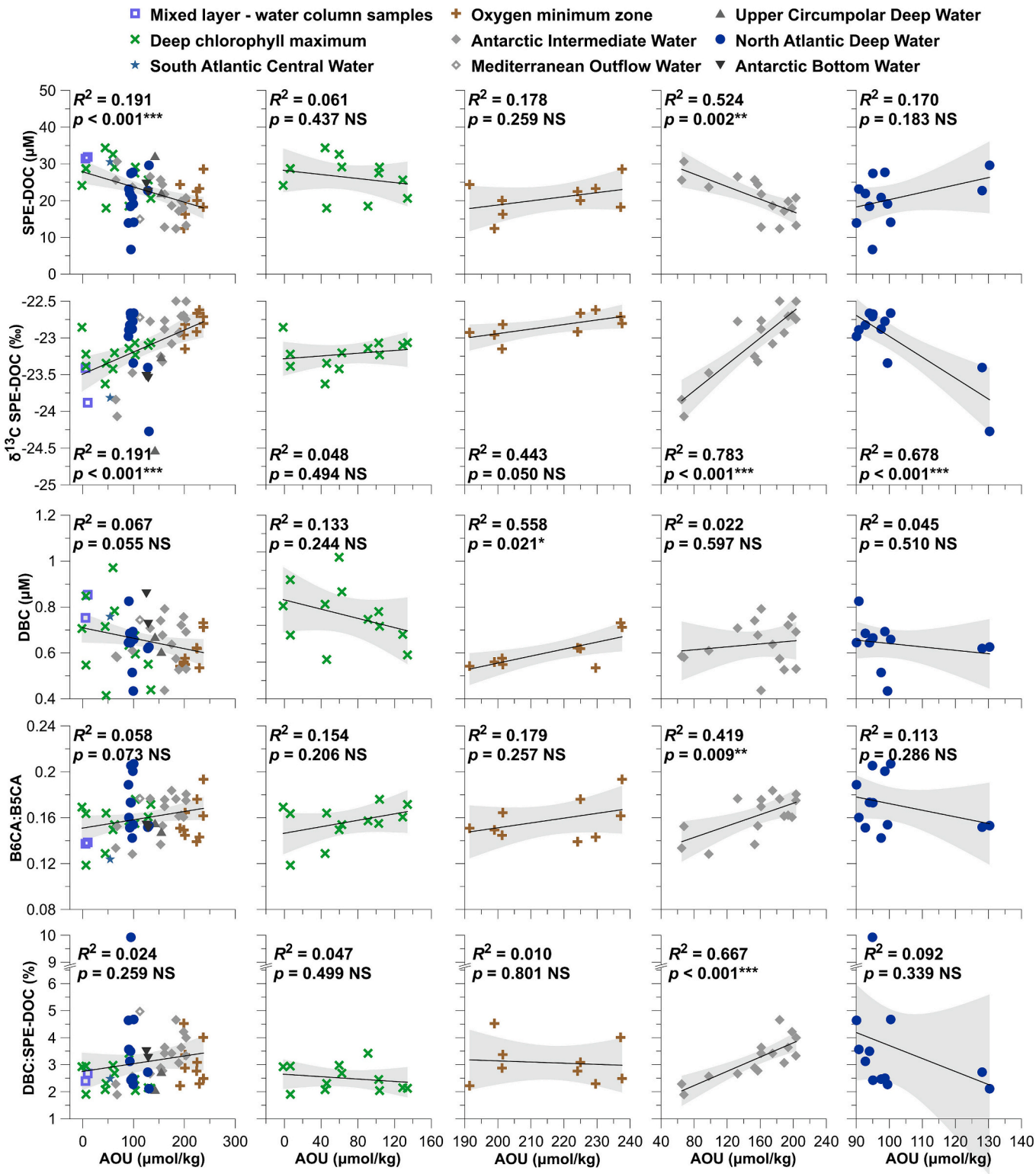

Fig. 6. Relationships between apparent oxygen utilization (AOU) and SPE-DOC and DBC properties in the Atlantic Ocean. From left to right, all water column samples, deep chlorophyll maximum, oxygen minimum zone, Antarctic Intermediate Water, and North Atlantic Deep Water. From top to bottom, SPE-DOC concentration and $\delta^{13}C$ composition and DBC concentration, degree of condensation (B6CA:B5CA molar ratio), and molar proportion in SPE-DOC. Grey shadings indicate the 95 % confidence intervals of the linear regressions. Determination R^2 coefficients and p-values for each linear regression are also shown, with their significance levels coded as follows: NS, not significant; *, $p < 0.05$; **, $p < 0.01$; and ***, $p < 0.001$.

The SPE fractionation thus preserves the main spatial trends (with one exception as discussed in Section 4.4.3) as depicted using the "bulk" DOC technology.

Our Atlantic SPE-DOC $\delta^{13}C$ values (−24.53 to −22.50 ‰) are similar to those of Wagner et al. (2019) from the same ocean at similar latitudes (−23.02 to −22.33 ‰) and coherent with DOC derived from marine phytoplankton (Beaupré, 2015). The Atlantic water profile of Wagner et al. (2019) also shows SPE-DOC $\delta^{13}C$ values heavier by ~0.5 ‰ in deep

waters compared with shallow waters, like most of our water column profiles. The tropical Atlantic Ocean consistently shows heavier SPE-DOC $\delta^{13}C$ values than does the higher latitude Zapiola Gyre off Argentina (Figs. 3c and 5). This latitudinal trend in SPE-DOC $\delta^{13}C$ values resembles those in $\delta^{13}C$ values for marine phytoplankton and particulate organic matter (Goericke and Fry, 1994; Fischer et al., 1998; Verwega et al., 2021). While the tropical Atlantic Ocean receives substantial atmospheric BC inputs with a ^{13}C-enriched signature (Cahoon et al., 1992; Eglinton et al., 2002; Randerson et al., 2005; Pohl et al., 2014; Global Modeling and Assimilation Office GMAO, 2015; van der Werf et al., 2017; Kirago et al., 2022; St Laurent et al., 2023), the small range in SPE-DOC $\delta^{13}C$ values (~2 ‰) detracts from meaningful C4 vegetation inputs to the oceanic DOC pool. In addition, our heaviest SPE-DOC $\delta^{13}C$ values within each of the most sampled water masses (surface waters, deep chlorophyll maximum, OMZ, AAIW, and NADW) occur towards 20°N rather than the equator (Fig. 5), similarly to particulate organic carbon $\delta^{13}C$ values in the Atlantic Ocean (Verwega et al., 2021). The significant correlation between SPE-DOC $\delta^{13}C$ and atmospheric BC column mass density thus does not likely show a causal relationship. Instead, the latitudinal covariation between our SPE-DOC $\delta^{13}C$ values and published particulate organic carbon $\delta^{13}C$ values (Fig. 5; Goericke and Fry, 1994; Fischer et al., 1998; Verwega et al., 2021) suggests that dissolved molecular CO_2 content is the main driver of not only particulate organic carbon $\delta^{13}C$ (Goericke and Fry, 1994; Fischer et al., 1998) but also SPE-DOC $\delta^{13}C$, assuming a constant isotopic SPE fractionation of oceanic DOC (Dulaquais et al., 2023 and references therein; caveats linked to the analysis of SPE-DOC rather than bulk-DOC properties discussed in Section 4.4.3). Overall, our SPE-DOC results suggest that oceanic DOC is essentially derived from marine phytoplankton, regardless the continental inputs from African savanna grassland fires to the Atlantic Ocean.

Our isotopic data suggest that the higher surface water SPE-DOC concentrations in the tropical Atlantic are not predominantly caused by substantial continental inputs from African savanna grassland fires. This is consistent with the occurrence of higher bulk-DOC concentrations in the tropics in all open oceans, even in regions that do not receive massive pyrogenic inputs (Hansell et al., 2009). In the Atlantic Ocean, atmospheric inputs from Africa would at most contribute to a subtle increase in surface water SPE-DOC concentrations towards the equator. Indeed, in the Santa Barbara Channel off California, the Thomas Fire smoke plume did not yield an increase in bulk-DOC and SPE-DOC concentrations despite the fire proximity and coastal context (Kelly et al., 2021; Wagner et al., 2021b). Alternatively, atmospheric inputs from Africa would not only supply BC, but also nutrients and trace metals among other elements to surface Atlantic waters. The airborne nutrients and trace metals delivered from Africa would then enhance phytoplankton production in surface Atlantic waters towards the equator. This alternative hypothesis appears reasonable, as the Thomas Fire smoke plume contained substantial amounts of trace metals (Kelly et al., 2021). The significant correlations between SPE-DOC concentration and atmospheric BC column mass density, notably in surface waters, thus most likely show indirect relationships.

4.2. Significance of atmospheric BC inputs from Africa as a source of DBC in the Atlantic Ocean

4.2.1. Further evidence of the ubiquity of oceanic DBC

All our seawater samples from the Atlantic Ocean yielded measurable BPCA amounts after SPE-DOC oxidation with HNO_3, regardless of atmospheric BC concentrations and despite the sampling away from major river mouths. Measured Atlantic Ocean DBC concentrations (0.4 to 1.0 μM) fall within the range of published DBC concentrations for open oceans (0.1 to 2.5 μM; Dittmar and Paeng, 2009; Ziolkowski and Druffel, 2010; Stubbins et al., 2012; Coppola and Druffel, 2016; Nakane et al., 2017; Wagner et al., 2017a, 2019; Fang et al., 2018b; Mori et al., 2021; Yamashita et al., 2022, 2023; Coppola et al., 2024). Similarly, measured DBC:SPE-DOC molar ratios (1 to 10 %) are similar to those calculated using published recoveries of SPE-DOC for open oceans (2 to 8 %; Stubbins et al., 2012; Coppola and Druffel, 2016; Fang et al., 2018b; Wagner et al., 2019; Coppola et al., 2024). Measured B6CA:B5CA ratios, all below 1, are consistent with published B6CA:B5CA ratios or those calculated from published B6CA and B5CA concentrations for open oceans (0.00 to 0.92; Stubbins et al., 2012; Wagner et al., 2017a, 2019; Fang et al., 2018b; Yamashita et al., 2022, 2023; Coppola et al., 2024).

4.2.2. Lack of atmospheric BC imprints from Africa on DBC in the Atlantic Ocean

Several previous studies supported the significance of atmospheric BC inputs as a non-riverine source of oceanic DBC, notably in open oceans (Jurado et al., 2008; Dittmar and Paeng, 2009; Bao et al., 2017, 2023; Nakane et al., 2017; Geng et al., 2021, 2023; Kelly et al., 2021; Mori et al., 2021; Wagner et al., 2021b; Yamashita et al., 2022, 2023; Zhang et al., 2024a). In the case of the tropical Atlantic Ocean, published data do not support this hypothesis (Ziolkowski and Druffel, 2010; Stubbins et al., 2012; Coppola and Druffel, 2016; Wagner et al., 2017a, 2019), as the highest reported DBC concentrations do not occur in areas with high inputs of pyrogenic materials as observed from satellite (Global Modeling and Assimilation Office GMAO, 2015; Buchard et al., 2017; Gelaro et al., 2017; Randles et al., 2017) and aerosol data (Virkkula et al., 2006). Furthermore, our DBC concentration values show little variability compared with major differences in the magnitude of pyrogenic inputs. For example, despite a five-fold increase in the atmospheric BC column mass density from the Zapiola Gyre off Argentina to the equator, no clear differences could be measured in DBC concentration (Figs. 2f and 3a and d). Similarly, we obtained low DBC:SPE-DOC molar ratios at all latitudes (<5 % except the NADW sample at PYRO22 ST06b due to a low SPE-DOC concentration value associated with an average DBC concentration value; Table S1), including in surface waters (Figs. 2i and 3f). Also, DBC:SPE-DOC ratios remain unchanged across the Atlantic Ocean (this study; Stubbins et al., 2012; Coppola and Druffel, 2016; Wagner et al., 2019), suggesting that no measurable incorporation of pyrogenic materials occur in this oceanic region. The lack of a coherent increase in DBC concentrations and DBC:SPE-DOC molar ratios from high-latitude regions to the equator in the Atlantic Ocean detracts from meaningful atmospheric BC imprints from the African Savanna on DBC in this ocean.

Given that atmospheric BC directly reaches surface waters but not deep waters, a focus on surface waters may provide clearer evidence for atmospheric BC imprints from Africa on DBC in the Atlantic Ocean. However, our surface water DBC concentration values do not peak towards the equator (Fig. 5), contrary to atmospheric BC column mass density values (Figs. 1 and 3a). Instead, surface water DBC concentrations subtly decrease from the South Atlantic to the tropical Atlantic Ocean, then sharply increase at the equator, and then remain constant in the Northern Hemisphere, resulting in a non-linear trend in DBC concentrations in surface Atlantic waters (Fig. 5). This is not the only study reporting the absence of correlation between atmospheric BC load and oceanic DBC concentration. Mari et al. (2017) did not observe an increase in DBC concentrations during the dry season despite the increase in atmospheric BC concentrations in Halong Bay, Vietnam. In the Santa Barbara Channel off California, Kelly et al. (2021) and Wagner et al. (2021b) reported subtle increases in surface water DBC concentrations due to the Thomas Fire smoke plume. In addition, the small ash-derived contributions from the Thomas Fire did not meaningfully shift the $\delta^{13}C$ signature of DBC beneath the smoke plume in the Santa Barbara Channel (Wagner et al., 2021b). Therefore, we do not expect a measurable ^{13}C enrichment of surface water DBC in the eastern equatorial Atlantic, given that no latitudinal trend was observed in DBC concentrations. Given that SPE-DOC and DBC concentrations are decoupled in surface waters ($n = 12$, $R^2 = 0.060$, $p = 0.444$; Fig. 7a), the absent relationship between atmospheric BC column mass density and DBC but not SPE-DOC concentration in surface Atlantic waters essentially reflects different geochemical processes, such as enhanced in situ production of

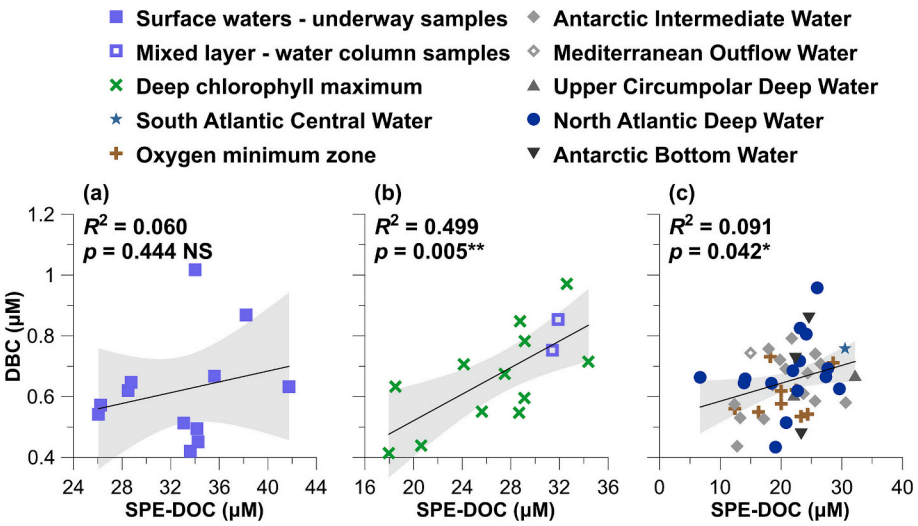

Fig. 7. Relationships between SPE-DOC and DBC properties in the Atlantic Ocean. (a) Surface waters, underway samples, (b) shallow waters, water column samples from the mixed layer and deep chlorophyll maximum, and (c) deep waters, water column samples deeper than the mixed layer and deep chlorophyll maximum. Grey shadings indicate the 95 % confidence intervals of the linear regressions. Determination R^2 coefficients and *p*-values for each linear regression are also shown, with their significance levels coded as follows: NS, not significant; *, $p < 0.05$; and **, $p < 0.01$.

DOC but not DBC from phytoplankton towards the equator.

Surface water B6CA:B5CA ratios show a decreasing trend from the South Atlantic to the tropical Atlantic Ocean, a trend which appears non-linear (Fig. 5) and is not significantly opposite to the latitudinal trend in surface water DBC concentrations ($n = 12$, $r = -0.419$, $p = 0.175$). This trend in B6CA:B5CA ratios in surface waters differs from what is observed in deeper water masses (as discussed in Sections 4.3.2, 4.3.3, 4.4.3, and 4.4.4), and suggests the existence of an additional DBC source, with relatively low B6CA:B5CA ratios, that modified the B6CA:B5CA ratios during the northward transport of Atlantic surface waters. A possible DBC source with lower B6CA:B5CA ratios in the South Atlantic may be wind-driven pyrogenic materials associated to African dust (Wagner et al., 2003). However, aged pyrogenic materials associated to dust tend to release DBC with high B6CA:B5CA ratios in contact with surface waters (Abiven et al., 2011; Wagner et al., 2017b, 2021b) and may yield an increase rather than a decrease in B6CA:B5CA ratios. Alternatively, the decrease in surface water B6CA:B5CA ratios from the South Atlantic to the tropical Atlantic Ocean may reflect stronger photo-bleaching of surface water DBC rather than enhanced atmospheric BC deposition in the tropics compared with higher latitude regions (Stubbins et al., 2012). The photo-bleaching hypothesis could be the most plausible one, as it may also explain the relatively small variability in surface water DBC concentrations compared to the large changes in atmospheric BC column mass density in the Atlantic Ocean. Given that atmospheric BC column mass density and solar radiation covary with latitude in the Atlantic Ocean, the constant DBC concentrations in surface Atlantic waters along latitude may be due to a balance between sources (e.g., atmospheric BC from Africa) and sinks (e.g., photo-bleaching) for Atlantic Ocean DBC, with an increase in both DBC supply and removal from high to low latitude regions. In conclusion, observed trends in surface water B6CA:B5CA ratios do not suggest measurable atmospheric BC imprints from the African Savanna on DBC in the Atlantic Ocean.

4.2.3. A link between atmospheric BC inputs from Africa and sedimentary BC in the Atlantic Ocean via particulate BC?

The Atlantic Ocean may capture the enhanced regional atmospheric BC deposition from African savanna grassland fires from the particulate rather than dissolved BC perspective. First, ash-derived contributions from the African Savanna may have remained undissolved into Atlantic waters (Abiven et al., 2011; Wagner et al., 2017b), undergone photo-bleaching (Stubbins et al., 2012), and/or been removed from the dissolved fraction from adsorption onto sinking particles (Coppola et al., 2014; Yamashita et al., 2022). Second, pelagic sediments from the Atlantic Ocean show a coherent maximum in BC concentrations and $\delta^{13}C$ values towards the equator and close to Africa (Niger Delta, Senegal Delta, and Sierra Leone Rise) and this sedimentary BC shows a larger modern fraction compared to the bulk total organic carbon in the same sediments (St Laurent et al., 2023; Katz et al., 2024). Third, Penalva Arias (2024) obtained using the BPCA method sedimentary BC patterns, notably B6CA and B5CA $\delta^{13}C$ values, which are coherent with the sedimentary BC patterns found by St Laurent et al. (2023) and Katz et al. (2024) using the chemothermal oxidation method. Fourth, Penalva Arias (2024) obtained sedimentary B6CA/B5CA ratios systematically above 1 in the Atlantic Ocean, contrary to our Atlantic water B6CA:B5CA molar ratios which are all below 1 (see B6CA and B5CA peak areas in Fig. S4), which provides further evidence for likely contrasting BC sources in Atlantic waters and sediments. Indeed, Coppola et al. (2014) found similar BPCA-based DBC condensation degrees for marine particulate and sedimentary BC, which are themselves more condensed than is DBC. Future studies using BC time series from sediment traps would help to assess our proposed links between the enhanced regional atmospheric BC deposition from African savanna grassland fires and the enhanced sedimentary BC content and its ^{13}C enrichment in the Atlantic Ocean.

4.3. Water depth and latitudinal changes in deep-water DBC concentration and condensation degree in the Atlantic Ocean

As described in Section 2.2, the sampling process was specifically designed to identify and sample the main existing deep Atlantic water masses to identify possible differences between water masses originating in distant locations. Accordingly, several samples were obtained to characterize DBC properties of each deep water mass (e.g., NADW, AAIW, AABW, and MOW), at different latitudes, and times (2021 and 2022). Subsurface waters within and below the chlorophyll maximum and the oxygen minima were also identified and sampled.

4.3.1. Uniform DBC concentration and variable DBC condensation degree in the Atlantic Ocean water column

DBC concentrations remain relatively constant across all deep water masses present in the Atlantic Ocean (Figs. 3d and 4a and c). Statistical

analyses based on principal component analysis (PCA) did not suggest any covariation between DBC concentration and environmental variables typically used to identify deep water masses (e.g., salinity and temperature; Figs. 4b and S7b). Also, other measured geochemical parameters (e.g., SPE-DOC concentration and $\delta^{13}C$ and B6CA:B5CA ratio) included in the PCA analysis showed weak to absent correlations with DBC concentration (Fig. 4b). By contrast, our PCA highlighted coherent changes in SPE-DOC properties (concentration and $\delta^{13}C$ composition) with water depth (as discussed in Section 4.1) and an anti-correlation between SPE-DOC concentration and DBC:SPE-DOC molar ratio ($n = 72$, $r = -0.731$, $p < 0.001$; Fig. 4b). This correlation was also significant when restricting the dataset to shallow and deep waters ($n = 60$, $r = -0.708$, $p < 0.001$; Fig. S7b). Overall, DBC concentrations provide little water mass characterization in the Atlantic Ocean. This general conclusion confirms previously reported water profiles in the Atlantic and Pacific Oceans (Wagner et al., 2019; Coppola et al., 2024) that show uniform DBC concentration patterns with water depth.

The only consistent changes in DBC properties with water depth are an increase in B6CA:B5CA molar ratios from surface waters to shallow and deep waters (Figs. 3e and 4; Table 1) and an increase in DBC:SPE-DOC molar ratios driven by a decrease in SPE-DOC concentrations from the first 1000 m to deeper waters (Figs. 3f and 4; Table 1). Again, these trends are similar to those reported by Wagner et al. (2019) and Coppola et al. (2024). Lower B6CA:B5CA and DBC:SPE-DOC molar ratios in surface waters than in deep waters may reflect photo-bleaching of DBC (Stubbins et al., 2012) and in situ production of DOC but not DBC from phytoplankton in surface waters. Water profiles across the Pacific Ocean revealed surface waters with typically higher DBC concentrations and lower BPCA-based DBC condensation degrees relative to deeper waters, possibly due to atmospheric BC deposition, preferential adsorption of the most condensed fraction of DBC onto sinking particles, DBC photo-bleaching, and anthropogenic soot deposition (Yamashita et al., 2022, 2023; Zhang et al., 2024a). In the North Pacific, Mori et al. (2021) found modest decreases in DBC concentrations from the surface layer (≤200 dbar) to deeper layers, which they attributed to atmospheric BC deposition, but an increase in BPCA-based DBC condensation degrees with water depth only within the surface layer due to dense shelf water influences in deeper layers, especially the intermediate layer (400–1000 dbar). Zhang et al. (2024a) also proposed dense shelf water influences on intermediate water DBC to explain the contrasting DBC distributions between intermediate waters and surface and subsurface waters in the Northwestern Pacific. In the Prydz Bay within the Southern Ocean, Fang et al. (2018b) found higher DBC concentrations in dense shelf waters than in environmental deep Antarctic waters, which themselves show DBC concentration values similar to ours in UCDW and AABW. In the Southern Ocean, Dittmar and Paeng (2009) found little variability in DBC concentrations between South Africa and Antarctica, with slightly higher DBC concentrations in subtropical surface waters, possibly due to atmospheric BC deposition and riverine inputs, and slightly lower DBC concentrations in Antarctic surface waters and AAIW. Yamashita et al. (2022) also found lower DBC concentrations in AAIW compared with surrounding Pacific waters, a trend which they attributed to photo-bleaching but is not visible in our Atlantic dataset.

Ziolkowski and Druffel (2010), Coppola and Druffel (2016), and Coppola et al. (2024) collectively reported ^{14}C ages from roughly 2500 to 23,000 ^{14}C years for oceanic DBC, which support the commonly admitted (ultra) recalcitrance of DBC. The (ultra) recalcitrance of DBC is a possible reason for the expectedly subtle to absent changes in open ocean DBC properties (Dittmar and Paeng, 2009). In addition to decoupled SPE-DOC and DBC concentrations in surface waters (as discussed in Section 4.2.2), our deep-water dataset (water column samples deeper than the mixed layer and deep chlorophyll maximum) shows a subtle relationship between SPE-DOC and DBC concentrations ($n = 46$, $R^2 = 0.091$, $p < 0.042$; Fig. 7c). This subtle relationship further demonstrates that SPE-DOC and DBC mostly experience contrasting geochemical processes, a contrast that may reflect the (ultra) recalcitrance of DBC compared with SPE-DOC, including its recalcitrant fraction (as discussed in Section 4.1). Yet, shallow waters (mixed layer and deep chlorophyll maximum) show a modest relationship between SPE-DOC and DBC concentrations ($n = 14$, $R^2 = 0.499$, $p < 0.005$; Fig. 7b). Modest anti-correlations were observed between atmospheric BC column mass density and both SPE-DOC ($n = 14$, $r = -0.610$, $p < 0.020$; Fig. 2b) and DBC concentrations ($n = 14$, $r = -0.594$, $p < 0.025$; Fig. 2f), suggesting that increased atmospheric inputs may reduce SPE-DOC and DBC concentrations in shallow waters. One hypothesis to explain this unexpected finding is that atmospheric inputs from Africa could enhance phytoplankton production (as discussed in Section 4.1), leading to enhanced adsorption of SPE-DOC and DBC onto sinking particles and their subsequent removal from shallow waters (Coppola et al., 2014; Yamashita et al., 2022). Indeed, recently published ^{14}C measurements on size-fractionated DBC revealed a cycling more dynamic and heterogeneous than previously believed (Coppola et al., 2024). Overall, the subtle to absent changes in oceanic DBC properties between the different water masses in the Atlantic Ocean are coherent with the (ultra-)recalcitrant nature of oceanic DBC, so future ^{14}C measurements on DBC within specific water masses may be necessary to properly characterize them from the oceanic DBC perspective.

4.3.2. *Lack of latitudinal variability in DBC concentration but not condensation degree in deep Atlantic waters*

Our DBC dataset shows subtle to absent latitudinal trends in DBC properties (Fig. 3d–f). When examining individual water masses—from shallow to deep waters—including the deep chlorophyll maximum, OMZ, AAIW, and NADW, DBC concentrations exhibit little latitudinal variability (Fig. 5). This pattern is consistent with surface water samples and remains evident even for AAIW and NADW. By contrast, Yamashita et al. (2022) found a gradual decrease in DBC concentrations along with meridional circulation in the deep Pacific Ocean. Given the anti-correlation between DBC concentration and AOU, Yamashita et al. (2022) attributed their results to DBC removal from adsorption onto sinking particles (Coppola et al., 2014). In the deep Atlantic Ocean and its individual shallow to deep water masses, DBC concentration and AOU did not show any anti-correlation (Fig. 6), which may be due to a balance between DBC removal from adsorption onto sinking particles and DBC sources that are likely not restricted to atmospheric BC inputs from Africa.

Along two other zonal and latitudinal transects across the Pacific Ocean, Yamashita et al. (2023) reported coherent changes in DBC concentrations but no correlation between DBC concentration and AOU, a deviation which they attributed to hydrothermal inputs that produce recalcitrant, aromatic-rich organic matter as a source of BPCAs from oxidation with HNO_3 (Dittmar and Koch, 2006; Rossel et al., 2017; Druffel et al., 2021; Brünjes et al., 2025). However, hydrothermal vents may also contribute to recalcitrant DOC removal and thus possibly to DBC removal from deep-sea waters (Hawkes et al., 2015). Future measurements of specific geochemical indicators (e.g., excess ^{3}He) would help to assess the influences of hydrothermal vents on DBC in deep Atlantic waters.

Sediment resuspension is another potential non-riverine source of deep-water DBC (Wagner et al., 2019), which may explain the lack of a gradual decrease in DBC concentrations along with meridional circulation in the deep Atlantic Ocean. Indeed, sediment resuspension may yield increased DBC concentrations in dense shelf waters compared with environmental deep water masses (Fang et al., 2018b; Mori et al., 2021; Zhang et al., 2024a). However, our DBC concentration profiles only show subtle changes with water depth (Figs. 3d and S5), which would detract from meaningful dense shelf water inputs. In addition, we took the deepest seawater samples in each profile from 149 to 1886 m above the bottom (Table S1) and found no relationship between DBC concentration and distance from the bottom for these seawater samples. Overall, we cannot attribute the lack of latitudinal changes in deep-water Atlantic DBC concentrations to sediment resuspension and

dense shelf water inputs.

When considering individual water masses separately, a consistent northward increasing trend in B6CA:B5CA ratios is apparent (Fig. 5), suggesting a northward increase in the condensation degree of DBC across the Atlantic Ocean. Yamashita et al. (2022) found an anti-correlation between BPCA-based DBC condensation degree and AOU in the deep Pacific Ocean, a trend which they attributed to the preferential adsorption of the most condensed fraction of DBC—producing B6CA and B5CA—onto sinking particles (Coppola et al., 2014). The DBC dataset of Yamashita et al. (2022) also shows a gradual decrease in B6CA:B5CA ratios—calculated from the published B6CA and B5CA concentration values—along with meridional circulation, suggesting a preferential adsorption of the B6CA-producing fraction of DBC onto sinking particles. In our study, the absent covariation between B6CA:B5CA ratio and AOU, and the correlation rather than anti-correlation between B6CA:B5CA ratio and AOU in AAIW (Fig. 6) further support the need to consider the balance between DBC sources and sinks in the deep Atlantic Ocean. For instance, the correlation between B6CA:B5CA ratio and fluorescence in shallow waters ($n = 14$, $r = 0.591$, $p < 0.026$) would not only explain the northward increase in B6CA:B5CA ratios within the deep chlorophyll maximum (Fig. 5), given the latitudinal trend in fluorescence (Fig. S2), but also suggest an additional DBC source with relatively high B6CA:B5CA ratios that would be enhanced under the upwelling conditions off Mauritania.

4.3.3. *Typically absent or indirect relationships between SPE-DOC and DBC properties and AOU–DO content in deep Atlantic waters*

The absent relationships with AOU–DO content are not restricted to DBC concentration but also apply to most other SPE-DOC and DBC properties and water masses in our Atlantic dataset, except for AAIW (Figs. 6 and S8). The general relationships between SPE-DOC properties and AOU–DO content are partly attributable to water column variations in SPE-DOC properties and AOU–DO content, which justifies a focus on individual water masses. When assuming a predominant marine phytoplankton source for SPE-DOC (as discussed in Section 4.1), the relationships between SPE-DOC $\delta^{13}C$ and AOU–DO content within AAIW and NADW (Figs. 6 and S8), as well as the relationship between SPE-DOC $\delta^{13}C$ and DO content within the OMZ (Fig. S8), may be linked to latitudinal trends in SPE-DOC $\delta^{13}C$ and AOU–DO content between 47°S and 29°N (Figs. 5 and S2). Indeed, our lightest SPE-DOC $\delta^{13}C$ values are associated to waters with relatively high dissolved molecular CO_2 content in the Southern Ocean (Goericke and Fry, 1994; Fischer et al., 1998), which correspond to relatively young AAIW (lowest AAIW AOU and highest AAIW DO content) and aged NADW (highest NADW AOU and lowest NADW DO content). Our heaviest SPE-DOC $\delta^{13}C$ values are associated to relatively young NADW (lowest NADW AOU and highest NADW DO content) and aged AAIW with AOU further increased and DO concentrations further reduced under the upwelling conditions off Mauritania that generate the OMZ.

Similarly, the relationships between B6CA:B5CA ratio and AOU–DO content in AAIW (Figs. 6 and S8) may essentially be associated to latitudinal trends in B6CA:B5CA ratios and AOU–DO content (Figs. 5 and S2). Alternatively, an additional DBC source with relatively high B6CA:B5CA ratios and possibly linked to atmospheric BC inputs ($n = 15$, $r = 0.552$, $p < 0.033$) would exceed the preferential removal of the B6CA-producing fraction of DBC but not the removal of DBC in general from adsorption onto sinking particles. This additional source would contribute to the balance between DBC sources and sinks and explain the correlation rather than anti-correlation between B6CA:B5CA ratio and AOU–DO in AAIW (as discussed in Section 4.3.2, with two other alternative hypotheses as discussed in Section 4.4.4). Except for the modest correlation between DBC concentration with AOU within the OMZ (as discussed in Section 4.4.2), the few significant relationships between SPE-DOC and DBC properties and AOU–DO content may be at most indirect.

4.4. *Potential alternative sources of DBC in the Atlantic Ocean*

4.4.1. *An oceanic DBC of predominantly non-pyrogenic origin?*

Rather than peaking towards the equator, surface Atlantic waters tend to show higher DBC concentrations in the Northern Hemisphere than in the Southern Hemisphere (Fig. 5). Given the main conclusion of Section 4.2.2, we cannot attribute this pattern exclusively to the seasonal peak in atmospheric BC column mass density which occurs in the Northern Hemisphere during the season of sampling. Instead, the lack of meaningful atmospheric BC imprints from the African Savanna on DBC in the Atlantic Ocean motivates the consideration of non-pyrogenic materials as possible sources of BPCAs from oxidation with HNO_3 (Hindersmann and Achten, 2017; Chang et al., 2018; Goranov et al., 2021; Vaezzadeh et al., 2023; Yin et al., 2024).

Stubbins et al. (2012, 2015) found strong relationships between DBC concentration and aromatic-rich CDOM abundance (light absorption coefficients at 300 and 254 nm, respectively) during a photo-bleaching experiment on a NADW sample and in arctic rivers, respectively. Similarly, the DBC dataset by Zhang et al. (2024a) shows a covariation between DBC concentration and CDOM abundance (light absorption coefficient at 254 nm) in surface waters along a transect from the East China Sea shelf to the Northwest Pacific Ocean, as well as in water column profiles from the Northwest Pacific Ocean. Given that humic acids may generate BPCAs from oxidation with HNO_3 due to their polycondensed aromatic structures (Chang et al., 2018), the strong relationships between BPCA-derived DBC and CDOM may also be strong relationships between humic-like compounds and CDOM in terms of abundance. Indeed, oceanic CDOM, including its fluorescent fraction, comprises humic-like compounds among other refractory compounds (Coble, 1996, 2007; Nelson and Siegel, 2013; Dittmar and Stubbins, 2014). In surface Atlantic waters, abundances of CDOM and humic-like components of fluorescent dissolved organic matter (FDOM) show minimal values in tropical gyres, intermediate values in upwelling regions and the Southern Ocean, and maximal values in the subarctic North Atlantic (Siegel et al., 2002, 2005; Nelson et al., 2007, 2010; Catalá et al., 2016).

Given the lack of CDOM–FDOM measurements for this study, our surface water DBC concentration values and DBC:SPE-DOC molar ratios are compared with satellite-based abundances of CDOM [$a_{CDOM}(443)$] in surface waters (Garver and Siegel, 1997; Maritorena et al., 2002; NASA Goddard Space Flight Center, Ocean Ecology Laboratory, Ocean Biology Processing Group, 2022). Overall, DBC concentration and $a_{CDOM}(443)$ are decoupled in surface Atlantic waters, a decoupling which also applies to DBC:SPE-DOC molar ratio (Fig. S6). When inspecting latitudinal changes in $a_{CDOM}(443)$, DBC concentrations, and DBC:SPE-DOC molar ratios in detail, all three properties show the expected covariation from 48°S to 20°S, whereas latitudinal changes in $a_{CDOM}(443)$ differ from those in DBC concentrations and DBC:SPE-DOC molar ratios from 7°S to 30°N (Fig. S9). For instance, the peak in satellite-based $a_{CDOM}(443)$ towards 20°N does not coincide with our highest DBC concentration value and DBC:SPE-DOC molar ratio at 30°N (Fig. S9), but does coincide with increased measured surface water abundances of CDOM and humic-like components of FDOM off Mauritania due to increased primary productivity under upwelling conditions (Heller et al., 2013; Gómez-Letona et al., 2022). The contrasting trends between DBC concentration and $a_{CDOM}(443)$ may be partly due to a stronger photo-bleaching of DBC than of CDOM under the high solar radiation conditions of the tropical Atlantic (Stubbins et al., 2012) among other additional factors. Interestingly, the covariation between DBC concentration and B6CA:B5CA ratio linked to photo-bleaching occurs from 48°S to 20°S but not from 7°S to 30°N in surface waters (Fig. 5), which suggests that the upwelling conditions off Mauritania may still contribute to the latitudinal variability in DBC concentrations in surface Atlantic waters. To confidently confirm or discard the hypothesis of a mostly non-pyrogenic oceanic DBC, we recommend paired analyses of DBC and CDOM–FDOM as in Stubbins

et al. (2012, 2015) and Zhang et al. (2024a) in the future, not only in additional surface seawater samples but also in additional deep seawater samples.

4.4.2. Possible reasons for the contrasting trends in DBC properties across the Atlantic and Pacific Oceans

When assuming an oceanic DBC of predominantly non-pyrogenic origin (Section 4.4.1), we may attribute the contrast in latitudinal trends in deep-sea DBC concentrations between the Atlantic and Pacific Oceans to the contrasting deep-water processes between both oceans. The Pacific Ocean shows correlations between CDOM abundance and AOU and between the abundance of humic-like components of FDOM and AOU which are almost absent in the Atlantic Ocean (Nelson et al., 2007, 2010; Yamashita and Tanoue, 2008, 2009; Swan et al., 2009; Jørgensen et al., 2011). While the Pacific Ocean shows opposite rather than similar changes in CDOM–FDOM abundances and DBC concentrations along with meridional circulation (Yamashita and Tanoue, 2008, 2009; Swan et al., 2009; Yamashita et al., 2022), the Atlantic Ocean shows constant CDOM–FDOM abundances and DBC concentrations along with meridional circulation (Figs. 5 and 6; Nelson et al., 2007, 2010; Jørgensen et al., 2011). Therefore, even in the case of a refuted correlation between CDOM–FDOM abundance and DBC concentration in the ocean, oceanic CDOM–FDOM and DBC may still experience similar geochemical processes with contrasting impacts on these properties and/or different geochemical processes with similar relationships with AOU (e.g., in situ CDOM–FDOM microbial production and DBC adsorption onto sinking particles).

The Atlantic Ocean also shows relatively homogenous distributions of CDOM and humic-like components of FDOM in deep waters compared with the Pacific Ocean, with symmetric latitudinal patterns for the former that contrast with asymmetric latitudinal patterns for the latter (Nelson et al., 2007, 2010; Yamashita and Tanoue, 2008, 2009; Swan et al., 2009; Catalá et al., 2015a, 2015b, 2016). These latitudinal changes in abundances of CDOM and humic-like components of FDOM in deep waters somehow resemble those in DBC concentration values from our study (Figs. 3d and 5) and from Yamashita et al. (2022) in the Atlantic and Pacific Oceans, respectively, although the latitudinal changes in CDOM–FDOM abundances and DBC concentrations are opposite in the Pacific Ocean. The opposite latitudinal changes in CDOM–FDOM abundances and DBC concentrations across the Pacific Ocean were attributed to in situ production of CDOM–FDOM from microbes (Yamashita and Tanoue, 2008, 2009; Swan et al., 2009) and DBC removal from adsorption onto sinking particles (Yamashita et al., 2022). Alternatively, microbes would produce both CDOM–FDOM and DBC, but DBC would subsequently experience a stronger removal from adsorption onto sinking particles than would CDOM–FDOM, resulting in a positive and negative net balance between sources and sinks for CDOM–FDOM and DBC, respectively, a hypothesis worth investigating in the future by following the research direction stated in Section 4.4.1.

Intermediate and deep waters in the Atlantic Ocean carry high-CDOM/low-AOU signals coupled to rapid overturning, whereas the same water layers in the Pacific Ocean carry low-CDOM/low-AOU signals coupled to autochthonous CDOM production and gradual increases in AOU (Nelson and Siegel, 2013). The high-CDOM/low-AOU signals in the Atlantic Ocean are partly due to the high abundances of CDOM and humic-like components of FDOM in the North Atlantic that NADW carry out across the Atlantic Ocean, given the substantial terrigenous inputs from surrounding continents and Arctic Ocean associated to limited photo-bleaching, greater mixing, and higher biological productivity (Opsahl et al., 1999; Amon et al., 2003; Benner et al., 2005; Jørgensen et al., 2011; Catalá et al., 2015a). Off Mauritania, the upwelling conditions yield increases in both abundances of humic-like components of FDOM and AOU, although the coupling remains imperfect due to terrestrial FDOM inputs which NADW carry from their source region (Heller et al., 2013; Catalá et al., 2015a, 2016; Gómez-Letona et al., 2022). While our dataset does not show an increase in deep-water DBC concentrations attributable to upwelling conditions off Mauritania (Fig. 3d), it does show a correlation between DBC concentration and AOU within the OMZ (Fig. 6). Upwelling conditions off Mauritania may thus enhance the production of both FDOM and DBC and thus contribute to the balance between DBC sources and sinks in the Atlantic Ocean (as discussed in Section 4.3.2). Overall, the consideration of relationships between concentrations of BPCA-derived DBC and abundances of CDOM and humic-like components of FDOM, as well as the export of chromophoric and fluorescent humic-like compounds from the North Atlantic by NADW, in addition to the balance between DBC production in upwelling systems and DBC removal from sinking particles, may explain the lack of latitudinal trends in DBC concentrations in deep Atlantic waters.

4.4.3. A connection between abundant terrestrial organic matter in the North Atlantic and DBC signals in deep Atlantic waters?

The substantial terrestrial inputs to the North Atlantic and their subsequent partial export by NADW also yield relatively high bulk-DOC concentrations in the deep North Atlantic (Hansell and Carlson (1998); Hansell et al., 2009). However, our NADW SPE-DOC concentration values do not decrease along with meridional circulation (Figs. 5 and 6), differently from bulk-DOC concentration values (Hansell et al., 2009), possibly due to variable SPE fractionation (Dulaquais et al., 2023 and references therein) and recovery within our dataset. Our dataset also shows a decrease in AAIW SPE-DOC concentrations along with meridional circulation rather than the expected increase based on published bulk-DOC concentrations (Figs. 5 and 6; Hansell et al., 2009), possibly for similar reasons as those for contrasting changes in bulk-DOC and SPE-DOC concentrations in NADW. The increase in AAIW DBC:SPE-DOC molar ratios along with meridional circulation is essentially due to the decrease in SPE-DOC concentrations, as DBC concentrations are constant (Figs. 5 and 6).

Our B6CA:B5CA molar ratios tend to decrease from the North Atlantic to the South Atlantic in NADW (Fig. 5), which may support the hypothetical export of terrestrial DBC from the North Atlantic by NADW. Indeed, riverine DBC consistently shows higher B6CA:B5CA molar ratios than does oceanic DBC (Wagner et al., 2019). However, the heavier rather than lighter SPE-DOC $\delta^{13}C$ values towards the north in all water masses (Fig. 5), when interpreted in terms of terrestrial contributions, would challenge the export of terrestrial DOC, including the DBC fraction, from the North Atlantic by NADW and support, for instance, the export of terrestrial DOC from the Southern Ocean by AAIW. Yet, B6CA:B5CA molar ratios in AAIW tend to increase rather than decrease from the South Atlantic to the North Atlantic (Fig. 5), which does not support a meaningful export of terrestrial DBC and possibly DOC as well from the Southern Ocean by AAIW. When assuming a predominant marine phytoplankton source for SPE-DOC (as discussed in Section 4.1), higher dissolved molecular CO_2 contents in the Southern Ocean than in the tropical Atlantic Ocean (Goericke and Fry, 1994; Fischer et al., 1998) would provide a more plausible reason for the heavier SPE-DOC $\delta^{13}C$ values towards the north in all water masses.

Accordingly, the shortcomings that would most likely challenge the hypothetical export of terrestrial DBC from the North Atlantic by NADW include the scarcity of SPE-DOC and DBC data from the North Atlantic at latitudes north from 30°N (Fig. S1), the assumption of a constant isotopic SPE fractionation of oceanic DOC (Dulaquais et al., 2023 and references therein), and the lack of DBC and BPCA-specific $\delta^{13}C$ data in the Atlantic Ocean (Wagner et al., 2019). Based on published particulate organic carbon $\delta^{13}C$ values, we may expect latitudinal trends towards lighter SPE-DOC $\delta^{13}C$ values from the tropical Atlantic to the North Atlantic (Goericke and Fry, 1994; Fischer et al., 1998; Verwega et al., 2021), a hypothesis worth testing by acquiring SPE-DOC $\delta^{13}C$ data along a latitudinal transect across the North Atlantic. The lack of a significant relationship between B6CA:B5CA and AOU in NADW may also challenge the export of terrestrial DBC from the North Atlantic by NADW, although NADW shows several missing AOU–DO values—due to data

processing—and a smaller range in AOU values (~40 μmol/kg) than does AAIW (~140 μmol/kg, Fig. 6). Future additional DBC latitudinal transects covering the entire Atlantic Ocean, notably the North Atlantic, would help to further test the hypothesis of a terrestrial DBC export from the North Atlantic by NADW.

4.4.4. Possible reasons for similar latitudinal changes in DBC properties despite meridional circulation from two contrasting sources

Despite their contrasting sources, AAIW and NADW show similar latitudinal trends in DBC concentrations and B6CA:B5CA ratios (Fig. 5). When assuming the export of terrestrial DBC from the North Atlantic by NADW (Section 4.4.3), the increase in AAIW B6CA:B5CA molar ratios along with meridional circulation (Figs. 5 and 6) may be due to a gradual mixing of AAIW into surrounding water masses from the North Atlantic (e.g., NADW), which would themselves carry DBC with relatively high B6CA:B5CA ratios. This explanation is consistent with the gradual increase in AAIW salinity along with meridional circulation (Fig. S2). Another possible reason for the lower AAIW B6CA:B5CA molar ratios in the South Atlantic than in the North Atlantic would imply lower B6CA:B5CA ratios in the Southern Ocean than in the Atlantic Ocean. Indeed, when inspecting B6CA:B5CA ratios calculated from the few published B6CA and B5CA concentrations from the Southern Ocean, the latitudinal transects of Fang et al. (2018b) and Yamashita et al. (2023) across the Prydz Bay and eastern South Pacific, respectively, show northward increases in B6CA:B5CA ratios. These latitudinal changes in B6CA:B5CA ratios suggest that AAIW would also carry DBC with relatively low B6CA:B5CA ratios, a hypothesis that remains to be established by examining DBC along latitudinal and longitudinal transects across the Southern Ocean, including the AAIW formation zone.

Further DBC studies in the Southern Ocean would also help to constrain the reasons why AAIW does not show lower DBC concentrations relative to surrounding water masses in the Atlantic Ocean, differently from the Southern and Pacific Oceans (Dittmar and Paeng, 2009; Yamashita et al., 2022). As discussed in Sections 4.3.2 and 4.3.3, an additional DBC source may not only balance DBC sinks (e.g., adsorption onto sinking particles), but also exceed a preferential removal of the B6CA-producing fraction of DBC from adsorption onto sinking particles in AAIW, although further work is required to confidently establish this DBC source. Overall, the non-systematic relationships of DBC properties with AOU within different water masses in the Atlantic Ocean support the need to consider additional, possibly non-pyrogenic sources of DBC in the future.

5. Conclusions

Our mapping of DBC in the Atlantic Ocean yields three main results. First, we do not observe meaningful imprints of enhanced regional atmospheric BC deposition from African savanna grassland fires on DBC in surface and deep Atlantic waters, likely due to enhanced DBC photobleaching towards the equator in surface waters. Second, DBC condensation degree but not concentration offers some characterization of specific water masses in the Atlantic Ocean, likely due to DBC photobleaching in surface waters. Third, DBC condensation degree but not concentration shows a northward increasing trend across the deep Atlantic Ocean. Our main results may be the consequence of 1) imprints of enhanced regional atmospheric BC deposition from African savanna grassland fires on particulate rather than dissolved BC in the Atlantic Ocean, 2) an (ultra-)refractory oceanic DBC of predominantly non-pyrogenic origin associated to a balance between additional DBC sources and main sinks in the Atlantic Ocean, and 3) exports of terrigenous humic-like compounds from the North Atlantic by NADW that may also be exports of terrigenous DBC across the Atlantic Ocean via meridional circulation.

CRediT authorship contribution statement

Nina Davtian: Validation, Funding acquisition, Data curation, Visualization, Investigation, Formal analysis, Writing – original draft. **Nuria Penalva:** Methodology, Data curation. **Oriol Teruel:** Data curation. **Pau Comes:** Data curation, Investigation. **Antoni Rosell-Melé:** Supervision, Funding acquisition, Conceptualization, Project administration, Data curation. **Joan Villanueva:** Project administration, Data curation, Supervision, Methodology, Conceptualization, Writing – review & editing.

Funding

This work was supported by the European Research Council (PALADYN Project #834934). ND is supported by the Juan de la Cierva Formación grant FJC2020-044864-I funded by MICIU/AEI/10.13039/501100011033 and by European Union NextGenerationEU/PRTR. JV is supported by the ICTA-UAB "María de Maeztu" Programme for Units of Excellence of the Spanish Ministry of Science and Innovation (CEX2019-000940-M) funded by MICIU/AEI/10.13039/501100011033.

Declaration of competing interest

The authors declare that they have no known competing financial interests or personal relationships that could have appeared to influence the work reported in this paper.

Acknowledgements

We thank the crew, marine technicians, and captains of the R/V Sarmiento de Gamboa and R/V Hesperides for their help with collecting the samples. We thank Alonso Hernández Guerra for the organization of the SAGA10W cruise to which ND, OT, and ARM participated for field sampling. Analyses and visualizations of atmospheric BC column mass density and surface water absorption due to CDOM and detrital material at 443 nm used in this paper were produced with the Giovanni online data system, developed and maintained by the NASA Goddard Earth Sciences Data and Information Services Center. We are grateful to two anonymous reviewers for their insightful comments that greatly helped us to improve this manuscript.

Appendix A. Supplementary data

Supplementary data to this article can be found online at https://doi.org/10.1016/j.marchem.2025.104568.

Data availability

All data generated from this study are presented in Figs. 2–5, S2, S3, and S5–S7 and Table 1. The dataset used for this study is available in Table S1. All PCA results are provided in Tables S2–S4.

References

Abernathey, R.P., Cerovecki, I., Holland, P.R., Newsom, E., Mazloff, M., Talley, L.D., 2016. Water-mass transformation by sea ice in the upper branch of the Southern Ocean overturning. Nat. Geosci. 9, 596–601. https://doi.org/10.1038/ngeo2749.

Abiven, S., Hengartner, P., Schneider, M.P.W., Singh, N., Schmidt, M.W.I., 2011. Pyrogenic carbon soluble fraction is larger and more aromatic in aged charcoal than in fresh charcoal. Soil Biol. Biochem. 43, 1615–1617. https://doi.org/10.1016/j.soilbio.2011.03.027.

Abney, R.B., Berhe, A.A., 2018. Pyrogenic carbon erosion: implications for stock and persistence of pyrogenic carbon in soil. Front. Earth Sci. 6, 26. https://doi.org/10.3389/feart.2018.00026.

Acker, J.G., Leptoukh, G., 2007. Online analysis enhances use of NASA Earth science data. EOS Trans. Am. Geophys. Union 88, 14–17. https://doi.org/10.1029/2007EO020003.

Álvarez, M., Brea, S., Mercier, H., Álvarez-Salgado, X.A., 2014. Mineralization of biogenic materials in the water masses of the South Atlantic Ocean. I: assessment and results of an optimum multiparameter analysis. Prog. Oceanogr. 123, 1–23. https://doi.org/10.1016/j.pocean.2013.12.007.

Ambar, I., Howe, M.R., 1979. Observations of the Mediterranean outflow—I mixing in the Mediterranean outflow. Deep-Sea Res. A Oceanogr. Res. Pap. 26, 535–554. https://doi.org/10.1016/0198-0149(79)90095-5.

Amon, R.M.W., Budéus, G., Meon, B., 2003. Dissolved organic carbon distribution and origin in the Nordic Seas: exchanges with the Arctic Ocean and the North Atlantic. J. Geophys. Res. Oceans 108, 3221. https://doi.org/10.1029/2002JC001594.

Bao, H., Niggemann, J., Luo, L., Dittmar, T., Kao, S.-J., 2017. Aerosols as a source of dissolved black carbon to the ocean. Nat. Commun. 8, 510. https://doi.org/10.1038/s41467-017-00437-3.

Bao, H., Niggemann, J., Du, M., Zhao, W., Huang, D., Yi, Y., Yang, J.-Y.T., Dittmar, T., Kao, S.-J., 2023. Deciphering sources and processing of dissolved black carbon in coastal seas. Limnol. Oceanogr. 68, 2562–2575. https://doi.org/10.1002/lno.12442.

Baringer, M.O., Price, J.F., 1997. Mixing and spreading of the Mediterranean outflow. J. Phys. Oceanogr. 27, 1654–1677. https://doi.org/10.1175/1520-0485(1997)027<1654:MASOTM>2.0.CO;2.

Barton, R., Richardson, C.M., Pae, E., Montalvo, M.S., Redmond, M., Zimmer, M.A., Wagner, S., 2024. Hydrology, rather than wildfire burn extent, determines post-fire organic and black carbon export from mountain rivers in central coastal California. Limnol. Oceanogr. Lett. 9, 70–80. https://doi.org/10.1002/lol2.10360.

Beaupré, S.R., 2015. Chapter 6 - the carbon isotopic composition of marine DOC. In: Hansell, D.A., Carlson, C.A. (Eds.), Biogeochemistry of Marine Dissolved Organic Matter, Second edition. Academic Press, Boston, pp. 335–368. https://doi.org/10.1016/B978-0-12-405940-5.00006-6.

Benner, R., Louchouarn, P., Amon, R.M.W., 2005. Terrigenous dissolved organic matter in the Arctic Ocean and its transport to surface and deep waters of the North Atlantic. Glob. Biogeochem. Cycles 19, GB2025. https://doi.org/10.1029/2004GB002398.

Bird, M.I., Wynn, J.G., Saiz, G., Wurster, C.M., McBeath, A., 2015. The pyrogenic carbon cycle. Annu. Rev. Earth Planet. Sci. 43, 273–298. https://doi.org/10.1146/annurev-earth-060614-105038.

Brünjes, J., Schubotz, F., Teske, A., Seidel, M., 2025. Molecular composition of dissolved organic matter from young organic-rich hydrothermal deep-sea sediments. Limnol. Oceanogr. Lett. https://doi.org/10.1002/lno.12812.

Buchard, V., Randles, C.A., da Silva, A.M., Darmenov, A., Colarco, P.R., Govindaraju, R., Ferrare, R., Hair, J., Beyersdorf, A.J., Ziemba, L.D., Yu, H., 2017. The MERRA-2 aerosol reanalysis, 1980 onward. Part II: evaluation and case studies. J. Clim. 30, 6851–6872. https://doi.org/10.1175/JCLI-D-16-0613.1.

Cahoon, D.R., Stocks, B.J., Levine, J.S., Cofer, W.R., O'Neill, K.P., 1992. Seasonal distribution of African savanna fires. Nature 359, 812–815. https://doi.org/10.1038/359812a0.

Cai, R., Jiao, N., 2023. Recalcitrant dissolved organic matter and its major production and removal processes in the ocean. Deep-Sea Res. I Oceanogr. Res. Pap. 191, 103922. https://doi.org/10.1016/j.dsr.2022.103922.

Carlson, C.A., Ducklow, H.W., 1995. Dissolved organic carbon in the upper ocean of the central equatorial Pacific Ocean, 1992: daily and finescale vertical variations. Deep-Sea Res. II Top. Stud. Oceanogr. 42, 639–656. https://doi.org/10.1016/0967-0645(95)00023-J.

Carracedo, L.I., Pardo, P.C., Flecha, S., Pérez, F.F., 2016. On the Mediterranean Water composition. J. Phys. Oceanogr. 46, 1339–1358. https://doi.org/10.1175/JPO-D-15-0095.1.

Catalá, T.S., Reche, I., Fuentes-Lema, A., Romera-Castillo, C., Nieto-Cid, M., Ortega-Retuerta, E., Calvo, E., Álvarez, M., Marrasé, C., Stedmon, C.A., Álvarez-Salgado, X.A., 2015a. Turnover time of fluorescent dissolved organic matter in the dark global ocean. Nat. Commun. 6, 5986. https://doi.org/10.1038/ncomms6986.

Catalá, T.S., Reche, I., Álvarez, M., Khatiwala, S., Guallart, E.F., Benítez-Barrios, V.M., Fuentes-Lema, A., Romera-Castillo, C., Nieto-Cid, M., Pelejero, C., Fraile-Nuez, E., Ortega-Retuerta, E., Marrasé, C., Álvarez-Salgado, X.A., 2015b. Water mass age and aging driving chromophoric dissolved organic matter in the dark global ocean. Glob. Biogeochem. Cycles 29, 917–934. https://doi.org/10.1002/2014GB005048.

Catalá, T.S., Álvarez-Salgado, X.A., Otero, J., Iuculano, F., Companys, B., Horstkotte, B., Romera-Castillo, C., Nieto-Cid, M., Latasa, M., Morán, X.A.G., Gasol, J.M., Marrasé, C., Stedmon, C.A., Reche, I., 2016. Drivers of fluorescent dissolved organic matter in the global epipelagic ocean. Limnol. Oceanogr. 61, 1101–1119. https://doi.org/10.1002/lno.10281.

Chang, Z., Tian, L., Li, F., Zhou, Y., Wu, M., Steinberg, C.E.W., Dong, X., Pan, B., Xing, B., 2018. Benzene polycarboxylic acid — a useful marker for condensed organic matter, but not for only pyrogenic black carbon. Sci. Total Environ. 626, 660–667. https://doi.org/10.1016/j.scitotenv.2018.01.145.

Coble, P.G., 1996. Characterization of marine and terrestrial DOM in seawater using excitation-emission matrix spectroscopy. Mar. Chem. 51, 325–346. https://doi.org/10.1016/0304-4203(95)00062-3.

Coble, P.G., 2007. Marine optical biogeochemistry: the chemistry of ocean color. Chem. Rev. 107, 402–418. https://doi.org/10.1021/cr050350+.

Coppola, A.I., Druffel, E.R.M., 2016. Cycling of black carbon in the ocean. Geophys. Res. Lett. 43, 4477–4482. https://doi.org/10.1002/2016GL068574.

Coppola, A.I., Ziolkowski, L.A., Masiello, C.A., Druffel, E.R.M., 2014. Aged black carbon in marine sediments and sinking particles. Geophys. Res. Lett. 41, 2427–2433. https://doi.org/10.1002/2013GL059068.

Coppola, A.I., Wiedemeier, D.B., Galy, V., Haghipour, N., Hanke, U.M., Nascimento, G.S., Usman, M., Blattmann, T.M., Reisser, M., Freymond, C.V., Zhao, M., Voss, B., Wacker, L., Schefuß, E., Peucker-Ehrenbrink, B., Abiven, S., Schmidt, M.W.I., Eglinton, T.I., 2018. Global-scale evidence for the refractory nature of riverine black carbon. Nat. Geosci. 11, 584–588. https://doi.org/10.1038/s41561-018-0159-8.

Coppola, A.I., Seidel, M., Ward, N.D., Viviroli, D., Nascimento, G.S., Haghipour, N., Revels, B.N., Abiven, S., Jones, M.W., Richey, J.E., Eglinton, T.I., Dittmar, T., Schmidt, M.W.I., 2019. Marked isotopic variability within and between the Amazon River and marine dissolved black carbon pools. Nat. Commun. 10, 4018. https://doi.org/10.1038/s41467-019-11543-9.

Coppola, A.I., Wagner, S., Lennartz, S.T., Seidel, M., Ward, N.D., Dittmar, T., Santín, C., Jones, M.W., 2022. The black carbon cycle and its role in the Earth system. Nat. Rev. Earth Environ. 3, 516–532. https://doi.org/10.1038/s43017-022-00316-6.

Coppola, A.I., Druffel, E.R.M., Broek, T.A., Haghipour, N., Eglinton, T.I., McCarthy, M., Walker, B.D., 2024. Variable aging and storage of dissolved black carbon in the ocean. Proc. Natl. Acad. Sci. USA 121, e2305030121. https://doi.org/10.1073/pnas.2305030121.

Dai, A., Trenberth, K.E., 2002. Estimates of freshwater discharge from continents: latitudinal and seasonal variations. J. Hydrometeorol. 3, 660–687. https://doi.org/10.1175/1525-7541(2002)003<0660:EOFDFC>2.0.CO;2.

Dickson, R.R., Brown, J., 1994. The production of North Atlantic Deep Water: sources, rates, and pathways. J. Geophys. Res. Oceans 99, 12319–12341. https://doi.org/10.1029/94JC00530.

Dittmar, T., 2008. The molecular level determination of black carbon in marine dissolved organic matter. Org. Geochem. 39, 396–407. https://doi.org/10.1016/j.orggeochem.2008.01.015.

Dittmar, T., Koch, B.P., 2006. Thermogenic organic matter dissolved in the abyssal ocean. Mar. Chem. 102, 208–217. https://doi.org/10.1016/j.marchem.2006.04.003.

Dittmar, T., Paeng, J., 2009. A heat-induced molecular signature in marine dissolved organic matter. Nat. Geosci. 2, 175–179. https://doi.org/10.1038/ngeo440.

Dittmar, T., Stubbins, A., 2014. 12.6 - dissolved organic matter in aquatic systems. In: Holland, H.D., Turekian, K.K. (Eds.), Treatise on Geochemistry, Second edition. Elsevier, Oxford, pp. 125–156. https://doi.org/10.1016/B978-0-08-095975-7.01010-X.

Dittmar, T., Koch, B., Hertkorn, N., Kattner, G., 2008. A simple and efficient method for the solid-phase extraction of dissolved organic matter (SPE-DOM) from seawater. Limnol. Oceanogr. Methods 6, 230–235. https://doi.org/10.4319/lom.2008.6.230.

Dittmar, T., Paeng, J., Gihring, T.M., Suryaputra, I.G.N.A., Huettel, M., 2012. Discharge of dissolved black carbon from a fire-affected intertidal system. Limnol. Oceanogr. 57, 1171–1181. https://doi.org/10.4319/lo.2012.57.4.1171.

Drake, T.W., Wagner, S., Stubbins, A., Wabakanghanzi, J.N., Dinga, J.B., Six, J., Spencer, R.G.M., 2020. Du Feu à l'Eau: source and flux of dissolved black carbon from the Congo River. Glob. Biogeochem. Cycles 34, e2020GB006560. https://doi.org/10.1029/2020GB006560.

Druffel, E.R.M., Griffin, S., Lewis, C.B., Rudresh, M., Garcia, N.G., Key, R.M., McNichol, A.P., Hauksson, N.E., Walker, B.D., 2021. Dissolved organic radiocarbon in the eastern Pacific and Southern Oceans. Geophys. Res. Lett. 48, e2021GL092904. https://doi.org/10.1029/2021GL092904.

Dulaquais, G., Fourrier, P., Maguer, J.F., Denis, C., Waeles, M., Riso, R., 2023. Size exclusion chromatography and stable carbon isotopes reveal the limitations of solid phase extraction with PPL to capture autochthonous DOM production. Mar. Chem. 249, 104213. https://doi.org/10.1016/j.marchem.2023.104213.

Eglinton, T.I., Eglinton, G., Dupont, L., Sholkovitz, E.R., Montluçon, D., Reddy, C.M., 2002. Composition, age, and provenance of organic matter in NW African dust over the Atlantic Ocean. Geochem. Geophys. Geosyst. 3, 1–27. https://doi.org/10.1029/2001GC000269.

Fang, Z., Yang, W., Chen, M., Ma, H., 2017. Source and fate of dissolved black carbon in the Western South China Sea during the Southwest monsoon prevailing season. J. Geophys. Res. Biogeosci. 122, 2817–2830. https://doi.org/10.1002/2017JG004014.

Fang, Y., Chen, Y., Tian, C., Wang, X., Lin, T., Hu, L., Li, J., Zhang, G., Luo, Y., 2018a. Cycling and budgets of organic and black carbon in coastal Bohai Sea, China: impacts of natural and anthropogenic perturbations. Glob. Biogeochem. Cycles 32, 971–986. https://doi.org/10.1029/2017GB005863.

Fang, Z., Yang, W., Chen, M., Stubbins, A., Ma, H., Jia, R., Li, Q., Chen, Q., 2018b. Transport of dissolved black carbon from the Prydz Bay shelf, Antarctica to the deep Southern Ocean. Limnol. Oceanogr. 63, 2179–2190. https://doi.org/10.1002/lno.10932.

Fang, Y., Chen, Y., Huang, G., Hu, L., Tian, C., Xie, J., Lin, J., Lin, T., 2021a. Particulate and dissolved black carbon in coastal China seas: spatiotemporal variations, dynamics, and potential implications. Environ. Sci. Technol. 55, 788–796. https://doi.org/10.1021/acs.est.0c06386.

Fang, Y., Huang, G., Chen, Y., Hu, L., Lin, J., Lin, T., 2021b. Particulate and dissolved black carbon in Bohai and Laizhou bays, China: distributions, sources, and contrasts under two distinct fluvial hydrological regimes. Front. Earth Sci. 9, 697728. https://doi.org/10.3389/feart.2021.697728.

Fang, Z., Yang, W., Stubbins, A., Chen, M., Li, J., Jia, R., Li, Q., Zhu, J., Wang, B., 2021c. Spatial characteristics and removal of dissolved black carbon in the western Arctic Ocean and Bering Sea. Geochim. Cosmochim. Acta 304, 178–190. https://doi.org/10.1016/j.gca.2021.04.024.

Fischer, G., Müller, P.J., Wefer, G., 1998. Latitudinal $\delta^{13}C_{org}$ variations in sinking matter and sediments from the South Atlantic: effects of anthropogenic CO_2 and implications for paleo-PCO_2 reconstructions. J. Mar. Syst. 17, 471–495. https://doi.org/10.1016/S0924-7963(98)00059-1.

Foldvik, A., Gammelsrød, T., 1988. Notes on Southern Ocean hydrography, sea-ice and bottom water formation. Palaeogeogr. Palaeoclimatol. Palaeoecol. 67, 3–17. https://doi.org/10.1016/0031-0182(88)90119-8.

Garver, S.A., Siegel, D.A., 1997. Inherent optical property inversion of ocean color spectra and its biogeochemical interpretation: 1. Time series from the Sargasso Sea. J. Geophys. Res. Oceans 102, 18607–18625. https://doi.org/10.1029/96JC03243.

Gelaro, R., McCarty, W., Suárez, M.J., Todling, R., Molod, A., Takacs, L., Randles, C.A., Darmenov, A., Bosilovich, M.G., Reichle, R., Wargan, K., Coy, L., Cullather, R., Draper, C., Akella, S., Buchard, V., Conaty, A., da Silva, A.M., Gu, W., Kim, G.-K., Koster, R., Lucchesi, R., Merkova, D., Nielsen, J.E., Partyka, G., Pawson, S., Putman, W., Rienecker, M., Schubert, S.D., Sienkiewicz, M., Zhao, B., 2017. The Modern-Era Retrospective Analysis for Research and Applications, version 2 (MERRA-2). J. Clim. 30, 5419–5454. https://doi.org/10.1175/JCLI-D-16-0758.1.

Geng, X., Zhong, G., Liu, J., Sun, Y., Yi, X., Bong, C.W., Zakaria, M.P., Gustafsson, Ö., Ouyang, Y., Zhang, G., 2021. Year-round measurements of dissolved black carbon in coastal Southeast Asia aerosols: rethinking its atmospheric deposition in the ocean. J. Geophys. Res. Atmos. 126, e2021JD034590. https://doi.org/10.1029/2021JD034590.

Geng, X., Haig, J., Lin, B., Tian, C., Zhu, S., Cheng, Z., Yuan, Y., Zhang, Y., Liu, J., Zheng, M., Li, J., Zhong, G., Zhao, S., Bird, M.I., Zhang, G., 2023. Provenance of aerosol black carbon over Northeast Indian Ocean and South China Sea and implications for oceanic black carbon cycling. Environ. Sci. Technol. 57, 13067–13078. https://doi.org/10.1021/acs.est.3c03481.

Glaser, B., Haumaier, L., Guggenberger, G., Zech, W., 1998. Black carbon in soils: the use of benzenecarboxylic acids as specific markers. Org. Geochem. 29, 811–819. https://doi.org/10.1016/S0146-6380(98)00194-6.

Global Modeling and Assimilation Office (GMAO), 2015. MERRA-2 tavgM_2d_aer_Nx: 2d, Monthly mean,Time-averaged,Single-Level,Assimilation,Aerosol Diagnostics V5.12.4. Goddard Earth Sciences Data and Information Services Center (GES DISC), Greenbelt, MD, USA. Accessed: 11 August 2023. http://doi.org/10.5067/FH9A0MLJPC7N.

Goericke, R., Fry, B., 1994. Variations of marine plankton $\delta^{13}C$ with latitude, temperature, and dissolved CO_2 in the world ocean. Glob. Biogeochem. Cycles 8, 85–90. https://doi.org/10.1029/93GB03272.

Goldberg, E.D., 1985. Black Carbon in the Environment: Properties and Distribution. John Wiley and Sons, New York, NY.

Gómez-Letona, M., Arístegui, J., Hernández-Hernández, N., Álvarez-Salgado, X.A., Álvarez, M., Delgadillo, E., Pérez-Lorenzo, M., Teira, E., Hernández-León, S., Sebastián, M., 2022. Deep ocean prokaryotes and fluorescent dissolved organic matter reflect the history of the water masses across the Atlantic Ocean. Prog. Oceanogr. 205, 102819. https://doi.org/10.1016/j.pocean.2022.102819.

Goranov, A.I., Schaller, M.F., Long, J.A., Podgorski, D.C., Wagner, S., 2021. Characterization of asphaltenes and petroleum using benzenepolycarboxylic acids (BPCAs) and compound-specific stable carbon isotopes. Energy Fuels 35, 18135–18145. https://doi.org/10.1021/acs.energyfuels.1c02374.

Gu, H., Liu, G., Wang, J., Aubry, A.-F., Arnold, M.E., 2014. Selecting the correct weighting factors for linear and quadratic calibration curves with least-squares regression algorithm in bioanalytical LC-MS/MS assays and impacts of using incorrect weighting factors on curve stability, data quality, and assay performance. Anal. Chem. 86, 8959–8966. https://doi.org/10.1021/ac5018265.

Hammes, K., Schmidt, M.W.I., Smernik, R.J., Currie, L.A., Ball, W.P., Nguyen, T.H., Louchouarn, P., Houel, S., Gustafsson, Ö., Elmquist, M., Cornelissen, G., Skjemstad, J.O., Masiello, C.A., Song, J., Peng, P., Mitra, S., Dunn, J.C., Hatcher, P.G., Hockaday, W.C., Smith, D.M., Hartkopf-Fröder, C., Böhmer, A., Lüer, B., Huebert, B.J., Amelung, W., Brodowski, S., Huang, L., Zhang, W., Gschwend, P.M., Flores-Cervantes, D.X., Largeau, C., Rouzaud, J.-N., Rumpel, C., Guggenberger, G., Kaiser, K., Rodionov, A., Gonzalez-Vila, F.J., Gonzalez-Perez, J.A., de la Rosa, J.M., Manning, D.A.C., López-Capél, E., Ding, L., 2007. Comparison of quantification methods to measure fire-derived (black/elemental) carbon in soils and sediments using reference materials from soil, water, sediment and the atmosphere. Glob. Biogeochem. Cycles 21, GB3016. https://doi.org/10.1029/2006GB002914.

Hansell, D.A., 2013. Recalcitrant dissolved organic carbon fractions. Annu. Rev. Mar. Sci. 5, 421–445. https://doi.org/10.1146/annurev-marine-120710-100757.

Hansell, D.A., Carlson, C.A., 1998. Deep-ocean gradients in the concentration of dissolved organic carbon. Nature 395, 263–266. https://doi.org/10.1038/26200.

Hansell, D.A., Carlson, C.A., 2001. Biogeochemistry of total organic carbon and nitrogen in the Sargasso Sea: control by convective overturn. Deep-Sea Res. II Top. Stud. Oceanogr. 48, 1649–1667. https://doi.org/10.1016/S0967-0645(00)00153-3.

Hansell, D., Carlson, C., Repeta, D., Schlitzer, R., 2009. Dissolved organic matter in the ocean: a controversy stimulates new insights. Oceanography 22, 202–211. https://doi.org/10.5670/oceanog.2009.109.

Hansell, D.A., Carlson, C.A., Schlitzer, R., 2012. Net removal of major marine dissolved organic carbon fractions in the subsurface ocean. Glob. Biogeochem. Cycles 26, GB1016. https://doi.org/10.1029/2011GB004069.

Hawkes, J.A., Rossel, P.E., Stubbins, A., Butterfield, D., Connelly, D.P., Achterberg, E.P., Koschinsky, A., Chavagnac, V., Hansen, C.T., Bach, W., Dittmar, T., 2015. Efficient removal of recalcitrant deep-ocean dissolved organic matter during hydrothermal circulation. Nat. Geosci. 8, 856–860. https://doi.org/10.1038/ngeo2543.

Hedges, J.I., Eglinton, G., Hatcher, P.G., Kirchman, D.L., Arnosti, C., Derenne, S., Evershed, R.P., Kögel-Knabner, I., de Leeuw, J.W., Littke, R., Michaelis, W., Rullkötter, J., 2000. The molecularly-uncharacterized component of nonliving organic matter in natural environments. Org. Geochem. 31, 945–958. https://doi.org/10.1016/S0146-6380(00)00096-6.

Heller, M.I., Gaiero, D.M., Croot, P.L., 2013. Basin scale survey of marine humic fluorescence in the Atlantic: relationship to iron solubility and H_2O_2. Glob. Biogeochem. Cycles 27, 88–100. https://doi.org/10.1029/2012GB004427.

Hindersmann, B., Achten, C., 2017. Accelerated benzene polycarboxylic acid analysis by liquid chromatography–time-of-flight–mass spectrometry for the determination of petrogenic and pyrogenic carbon. J. Chromatogr. A 1510, 57–65. https://doi.org/10.1016/j.chroma.2017.06.058.

Howell, D.C., 2010. Statistical Methods for Psychology, seventh. ed. Cengage Learning, Wadsworth.

Jaffé, R., Ding, Y., Niggemann, J., Vähätalo, A.V., Stubbins, A., Spencer, R.G.M., Campbell, J., Dittmar, T., 2013. Global charcoal mobilization from soils via dissolution and riverine transport to the oceans. Science 340, 345–347. https://doi.org/10.1126/science.1231476.

Jenkins, W.J., Smethie, W.M., Boyle, E.A., Cutter, G.A., 2015. Water mass analysis for the U.S. GEOTRACES (GA03) North Atlantic sections. Deep-Sea Res. II Top. Stud. Oceanogr. 116, 6–20. https://doi.org/10.1016/j.dsr2.2014.11.018.

Jones, M.W., de Aragão, L.E.O.C., Dittmar, T., de Rezende, C.E., Almeida, M.G., Johnson, B.T., Marques, J.S.J., Niggemann, J., Rangel, T.P., Quine, T.A., 2019. Environmental controls on the riverine export of dissolved black carbon. Glob. Biogeochem. Cycles 33, 849–874. https://doi.org/10.1029/2018GB006140.

Jones, M.W., Coppola, A.I., Santín, C., Dittmar, T., Jaffé, R., Doerr, S.H., Quine, T.A., 2020. Fires prime terrestrial organic carbon for riverine export to the global oceans. Nat. Commun. 11, 2791. https://doi.org/10.1038/s41467-020-16576-z.

Jørgensen, L., Stedmon, C.A., Kragh, T., Markager, S., Middelboe, M., Søndergaard, M., 2011. Global trends in the fluorescence characteristics and distribution of marine dissolved organic matter. Mar. Chem. 126, 139–148. https://doi.org/10.1016/j.marchem.2011.05.002.

Josse, J., Husson, F., 2016. missMDA: a package for handling missing values in multivariate data analysis. J. Stat. Softw. 70, 1–31. https://doi.org/10.18637/jss.v070.i01.

Jurado, E., Dachs, J., Duarte, C.M., Simó, R., 2008. Atmospheric deposition of organic and black carbon to the global oceans. Atmos. Environ. 42, 7931–7939. https://doi.org/10.1016/j.atmosenv.2008.07.029.

Kappenberg, A., Bläsing, M., Lehndorff, E., Amelung, W., 2016. Black carbon assessment using benzene polycarboxylic acids: limitations for organic-rich matrices. Org. Geochem. 94, 47–51. https://doi.org/10.1016/j.orggeochem.2016.01.009.

Karstensen, J., Stramma, L., Visbeck, M., 2008. Oxygen minimum zones in the eastern tropical Atlantic and Pacific oceans. Prog. Oceanogr. 77, 331–350. https://doi.org/10.1016/j.pocean.2007.05.009.

Kassambara, A., 2023. rstatix: Pipe-Friendly Framework for Basic Statistical Tests.

Katz, S.D., Kelly, R.P., Robinson, R.S., Pavia, F.J., Pockalny, R., Lohmann, R., 2024. Biomass burning is a source of modern black carbon to equatorial Atlantic Ocean sediments. Commun. Earth Environ. 5, 536. https://doi.org/10.1038/s43247-024-01642-x.

Kelly, R.L., Bian, X., Feakins, S.J., Fornace, K.L., Gunderson, T., Hawco, N.J., Liang, H., Niggemann, J., Paulson, S.E., Pinedo-Gonzalez, P., West, A.J., Yang, S.-C., John, S.G., 2021. Delivery of metals and dissolved black carbon to the southern California coastal ocean via aerosols and floodwaters following the 2017 Thomas Fire. J. Geophys. Res. Biogeosci. 126, e2020JG006117. https://doi.org/10.1029/2020JG006117.

Kirago, L., Gustafsson, Ö., Gaita, S.M., Haslett, S.L., deWitt, H.L., Gasore, J., Potter, K.E., Prinn, R.G., Rupakheti, M., de D Ndikubwimana, J., Safari, B., Andersson, A., 2022. Atmospheric black carbon loadings and sources over eastern sub-saharan Africa are governed by the regional savanna fires. Environ. Sci. Technol. 56, 15460–15469. https://doi.org/10.1021/acs.est.2c05837.

Kirchner, K., Rhein, M., Hüttl-Kabus, S., Böning, C.W., 2009. On the spreading of South Atlantic Water into the Northern Hemisphere. J. Geophys. Res. Oceans 114, C05019. https://doi.org/10.1029/2008JC005165.

Kuhlbusch, T.A.J., Crutzen, P.J., 1995. Toward a global estimate of black carbon in residues of vegetation fires representing a sink of atmospheric CO_2 and a source of O_2. Glob. Biogeochem. Cycles 9, 491–501. https://doi.org/10.1029/95GB02742.

Kuo, L.-J., Louchouarn, P., Herbert, B.E., 2011. Influence of combustion conditions on yields of solvent-extractable anhydrosugars and lignin phenols in chars: implications for characterizations of biomass combustion residues. Chemosphere 85, 797–805. https://doi.org/10.1016/j.chemosphere.2011.06.074.

Lancelot, C., Fasham, M., Legendre, L., Radach, G., Scott, M., Kirchman, D.L., 1993. Dissolved organic matter in biogeochemical models of the ocean. In: Evans, G.T., Fasham, M.J.R. (Eds.), Towards a Model of Ocean Biogeochemical Processes. Springer, Berlin, Heidelberg, pp. 209–225. https://doi.org/10.1007/978-3-642-84602-1_10.

Lê, S., Josse, J., Husson, F., 2008. FactoMineR: an R package for multivariate analysis. J. Stat. Softw. 25, 1–18. https://doi.org/10.18637/jss.v025.i01.

Liu, M., Tanhua, T., 2021. Water masses in the Atlantic Ocean: characteristics and distributions. Ocean Sci. 17, 463–486. https://doi.org/10.5194/os-17-463-2021.

Mari, X., Chu Van, T., Guinot, B., Brune, J., Lefebvre, J.-P., Raimbault, P., Dittmar, T., Niggemann, J., 2017. Seasonal dynamics of atmospheric and river inputs of black carbon, and impacts on biogeochemical cycles in Halong Bay, Vietnam. Elem. Sci. Anth. 5, 75. https://doi.org/10.1525/elementa.255.

Maritorena, S., Siegel, D.A., Peterson, A.R., 2002. Optimization of a semianalytical ocean color model for global-scale applications. Appl. Opt. 41, 2705–2714. https://doi.org/10.1364/AO.41.002705.

Marshall, J., Speer, K., 2012. Closure of the meridional overturning circulation through Southern Ocean upwelling. Nat. Geosci. 5, 171–180. https://doi.org/10.1038/ngeo1391.

Masiello, C.A., 2004. New directions in black carbon organic geochemistry. Mar. Chem. 92, 201–213. https://doi.org/10.1016/j.marchem.2004.06.043.

Mercier, H., Arhan, M., Lutjeharms, J.R.E., 2003. Upper-layer circulation in the eastern Equatorial and South Atlantic Ocean in January–March 1995. Deep-Sea Res. I Oceanogr. Res. Pap. 50, 863–887. https://doi.org/10.1016/S0967-0637(03)00071-2.

Mitra, S., Zimmerman, A.R., Hunsinger, G., Woerner, W.R., 2013. Black carbon in coastal and large river systems. In: Allison, M.A., Bianchi, T.S., Cai, W.-J. (Eds.), Biogeochemical Dynamics at Major River-Coastal Interfaces: Linkages with Global Change. Cambridge University Press, Cambridge, pp. 200–234. https://doi.org/10.1017/CBO9781139136853.012.

Moran, M.A., Kujawinski, E.B., Stubbins, A., Fatland, R., Aluwihare, L.I., Buchan, A., Crump, B.C., Dorrestein, P.C., Dyhrman, S.T., Hess, N.J., Howe, B., Longnecker, K., Medeiros, P.M., Niggemann, J., Obernosterer, I., Repeta, D.J., Waldbauer, J.R., 2016. Deciphering ocean carbon in a changing world. Proc. Natl. Acad. Sci. USA 113, 3143–3151. https://doi.org/10.1073/pnas.1514645113.

Mori, Y., Nishioka, J., Fujio, S., Yamashita, Y., 2021. Transport of dissolved black carbon from marginal sea sediments to the western North Pacific. Prog. Oceanogr. 193, 102552. https://doi.org/10.1016/j.pocean.2021.102552.

Nakane, M., Ajioka, T., Yamashita, Y., 2017. Distribution and sources of dissolved black carbon in surface waters of the Chukchi Sea, Bering Sea, and the North Pacific Ocean. Front. Earth Sci. 5, 34. https://doi.org/10.3389/feart.2017.00034.

NASA Goddard Space Flight Center, Ocean Ecology Laboratory, Ocean Biology Processing Group, 2022. Sea-Viewing Wide Field-of-View Sensor (SeaWiFS) ORBVIEW-2 SeaWiFS Level-3 Mapped Inherent Optical Properties, Version 2022.0 Data. NASA OB.DAAC, Greenbelt, MD, USA. Accessed: 18 December 2024. http://doi.org/10.5067/ORBVIEW-2/SEAWIFS/L3M/IOP/2022.0.

Nelson, N.B., Siegel, D.A., 2013. The global distribution and dynamics of chromophoric dissolved organic matter. Annu. Rev. Mar. Sci. 5, 447–476. https://doi.org/10.1146/annurev-marine-120710-100751.

Nelson, N.B., Siegel, D.A., Carlson, C.A., Swan, C., Smethie, W.M., Khatiwala, S., 2007. Hydrography of chromophoric dissolved organic matter in the North Atlantic. Deep-Sea Res. I Oceanogr. Res. Pap. 54, 710–731. https://doi.org/10.1016/j.dsr.2007.02.006.

Nelson, N.B., Siegel, D.A., Carlson, C.A., Swan, C.M., 2010. Tracing global biogeochemical cycles and meridional overturning circulation using chromophoric dissolved organic matter. Geophys. Res. Lett. 37, L03610. https://doi.org/10.1029/2009GL042325.

Opsahl, S., Benner, R., Amon, R.M.W., 1999. Major flux of terrigenous dissolved organic matter through the Arctic Ocean. Limnol. Oceanogr. 44, 2017–2023. https://doi.org/10.4319/lo.1999.44.8.2017.

Orsi, A.H., Johnson, G.C., Bullister, J.L., 1999. Circulation, mixing, and production of Antarctic Bottom Water. Prog. Oceanogr. 43, 55–109. https://doi.org/10.1016/S0079-6611(99)00004-X.

Penalva Arias, N., 2024. Identification of Black Carbon Contributions in Oceanic Sediments using Benzene Polycarboxylic Acid Markers (Ph.D. Thesis). TDX (Tesis Doctorals en Xarxa). Universitat Autònoma de Barcelona. https://www.tdx.cat/handle/10803/692155.

Penalva-Arias, N., Teruel, O., Raja, M., Rosell-Melé, A., Villanueva, J., 2024. Quantification and isotopic characterization of benzene polycarboxylic acids (BPCA)-derived black carbon in deep oceanic sediments: towards assessing pyrogenic inputs from marine sources. Org. Geochem. 193, 104811. https://doi.org/10.1016/j.orggeochem.2024.104811.

Piola, A.R., Gordon, A.L., 1989. Intermediate waters in the southwest South Atlantic. Deep-Sea Res. A Oceanogr. Res. Pap. 36, 1–16. https://doi.org/10.1016/0198-0149(89)90015-0.

Pohl, K., Cantwell, M., Herckes, P., Lohmann, R., 2014. Black carbon concentrations and sources in the marine boundary layer of the tropical Atlantic Ocean using four methodologies. Atmos. Chem. Phys. 14, 7431–7443. https://doi.org/10.5194/acp-14-7431-2014.

Price, J.F., Baringer, M.O., Lueck, R.G., Johnson, G.C., Ambar, I., Parrilla, G., Cantos, A., Kennelly, M.A., Sanford, T.B., 1993. Mediterranean outflow mixing and dynamics. Science 259, 1277–1282. https://doi.org/10.1126/science.259.5099.1277.

Qi, Y., Fu, W., Tian, J., Luo, C., Shan, S., Sun, S., Ren, P., Zhang, H., Liu, J., Zhang, X., Wang, X., 2021. Reply to: "Questions remain about the biolability of dissolved black carbon along the combustion continuum". Nat. Commun. 12, 4282. https://doi.org/10.1038/s41467-021-24478-x.

R Core Team, 2024. R: A Language and Environment for Statistical Computing, Vienna, Austria.

Randerson, J.T., van der Werf, G.R., Collatz, G.J., Giglio, L., Still, C.J., Kasibhatla, P., Miller, J.B., White, J.W.C., DeFries, R.S., Kasischke, E.S., 2005. Fire emissions from C3 and C4 vegetation and their influence on interannual variability of atmospheric CO_2 and $\delta^{13}CO_2$. Glob. Biogeochem. Cycles 19, GB2019. https://doi.org/10.1029/2004GB002366.

Randles, C.A., da Silva, A.M., Buchard, V., Colarco, P.R., Darmenov, A., Govindaraju, R., Smirnov, A., Holben, B., Ferrare, R., Hair, J., Shinozuka, Y., Flynn, C.J., 2017. The MERRA-2 aerosol reanalysis, 1980 onward. Part I: system description and data assimilation evaluation. J. Clim. 30, 6823–6850. https://doi.org/10.1175/JCLI-D-16-0609.1.

Reid, J.L., 1978. On the middepth circulation and salinity field in the North Atlantic Ocean. J. Geophys. Res. Oceans 83, 5063–5067. https://doi.org/10.1029/JC083iC10p05063.

Reid, J.L., 1979. On the contribution of the Mediterranean Sea outflow to the Norwegian-Greenland Sea. Deep-Sea Res. A Oceanogr. Res. Pap. 26, 1199–1223. https://doi.org/10.1016/0198-0149(79)90064-5.

Reid, J.L., 1989. On the total geostrophic circulation of the South Atlantic Ocean: flow patterns, tracers, and transports. Prog. Oceanogr. 23, 149–244. https://doi.org/10.1016/0079-6611(89)90001-3.

Reid, J.L., 1994. On the total geostrophic circulation of the North Atlantic Ocean: flow patterns, tracers, and transports. Prog. Oceanogr. 33, 1–92. https://doi.org/10.1016/0079-6611(94)90014-0.

Rossel, P.E., Stubbins, A., Rebling, T., Koschinsky, A., Hawkes, J.A., Dittmar, T., 2017. Thermally altered marine dissolved organic matter in hydrothermal fluids. Org. Geochem. 110, 73–86. https://doi.org/10.1016/j.orggeochem.2017.05.003.

Roth, P.J., Lehndorff, E., Brodowski, S., Bornemann, L., Sanchez-García, L., Gustafsson, Ö., Amelung, W., 2012. Differentiation of charcoal, soot and diagenetic carbon in soil: method comparison and perspectives. Org. Geochem. 46, 66–75. https://doi.org/10.1016/j.orggeochem.2012.01.012.

Saenko, O.A., Weaver, A.J., 2001. Importance of wind-driven sea ice motion for the formation of Antarctic Intermediate Water in a global climate model. Geophys. Res. Lett. 28, 4147–4150. https://doi.org/10.1029/2001GL013632.

Santín, C., Doerr, S.H., Preston, C.M., González-Rodríguez, G., 2015. Pyrogenic organic matter production from wildfires: a missing sink in the global carbon cycle. Glob. Chang. Biol. 21, 1621–1633. https://doi.org/10.1111/gcb.12800.

Santín, C., Doerr, S.H., Kane, E.S., Masiello, C.A., Ohlson, M., de la Rosa, J.M., Preston, C.M., Dittmar, T., 2016. Towards a global assessment of pyrogenic carbon from vegetation fires. Glob. Chang. Biol. 22, 76–91. https://doi.org/10.1111/gcb.12985.

Schlitzer, R., 2024. Ocean Data View.

Schmidt, M.W.I., Noack, A.G., 2000. Black carbon in soils and sediments: analysis, distribution, implications, and current challenges. Glob. Biogeochem. Cycles 14, 777–793. https://doi.org/10.1029/1999GB001208.

Siedler, G., Müller, T.J., Onken, R., Arhan, M., Mercier, H., King, B.A., Saunders, P.M., 1996. The zonal WOCE sections in the South Atlantic. In: Wefer, G., Berger, W.H., Siedler, Gerold, Webb, D.J. (Eds.), The South Atlantic: Present and Past Circulation. Springer, Berlin, Heidelberg, pp. 83–104. https://doi.org/10.1007/978-3-642-80353-6_5.

Siegel, D.A., Maritorena, S., Nelson, N.B., Hansell, D.A., Lorenzi-Kayser, M., 2002. Global distribution and dynamics of colored dissolved and detrital organic materials. J. Geophys. Res. Oceans 107. https://doi.org/10.1029/2001JC000965, 21-1–21-14.

Siegel, D.A., Maritorena, S., Nelson, N.B., Behrenfeld, M.J., McClain, C.R., 2005. Colored dissolved organic matter and its influence on the satellite-based characterization of the ocean biosphere. Geophys. Res. Lett. 32, L20605. https://doi.org/10.1029/2005GL024310.

Speidel, L.G., Carvalho da Silva, R., Beck, M., Dellwig, O., Wollschläger, J., Dittmar, T., Seidel, M., 2024. Rivers and tidal flats as sources of dissolved organic matter and trace metals in the German Bight (North Sea). Biogeochemistry 167, 225–250. https://doi.org/10.1007/s10533-024-01117-3.

St Laurent, K., Cantwell, M., Lohmann, R., 2023. New insights on black carbon in pelagic Atlantic sediments. Mar. Chem. 257, 104312. https://doi.org/10.1016/j.marchem.2023.104312.

Stramma, L., England, M., 1999. On the water masses and mean circulation of the South Atlantic Ocean. J. Geophys. Res. Oceans 104, 20863–20883. https://doi.org/10.1029/1999JC900139.

Stramma, L., Kieke, D., Rhein, M., Schott, F., Yashayaev, I., Koltermann, K.P., 2004. Deep water changes at the western boundary of the subpolar North Atlantic during 1996 to 2001. Deep-Sea Res. I Oceanogr. Res. Pap. 51, 1033–1056. https://doi.org/10.1016/j.dsr.2004.04.001.

Stramma, L., Hüttl, S., Schafstall, J., 2005. Water masses and currents in the upper tropical northeast Atlantic off northwest Africa. J. Geophys. Res. Oceans 110, C12006. https://doi.org/10.1029/2005JC002939.

Stramma, L., Brandt, P., Schafstall, J., Schott, F., Fischer, J., Körtzinger, A., 2008. Oxygen minimum zone in the North Atlantic south and east of the Cape Verde Islands. J. Geophys. Res. Oceans 113, C04014. https://doi.org/10.1029/2007JC004369.

Stubbins, A., Niggemann, J., Dittmar, T., 2012. Photo-lability of deep ocean dissolved black carbon. Biogeosciences 9, 1661–1670. https://doi.org/10.5194/bg-9-1661-2012.

Stubbins, A., Spencer, R.G.M., Mann, P.J., Holmes, R.M., McClelland, J.W., Niggemann, J., Dittmar, T., 2015. Utilizing colored dissolved organic matter to derive dissolved black carbon export by arctic rivers. Front. Earth Sci. 3, 63. https://doi.org/10.3389/feart.2015.00063.

Swan, C.M., Siegel, D.A., Nelson, N.B., Carlson, C.A., Nasir, E., 2009. Biogeochemical and hydrographic controls on chromophoric dissolved organic matter distribution in the Pacific Ocean. Deep-Sea Res. I Oceanogr. Res. Pap. 56, 2175–2192. https://doi.org/10.1016/j.dsr.2009.09.002.

Talley, L.D., 1996. Antarctic Intermediate Water in the South Atlantic. In: Wefer, G., Berger, W.H., Siedler, G., Webb, D.J. (Eds.), The South Atlantic: Present and Past Circulation. Springer, Berlin, Heidelberg, pp. 219–238. https://doi.org/10.1007/978-3-642-80353-6_11.

Tomczak, M., Godfrey, J.S., 1994. Regional Oceanography: An Introduction, 1st ed. Pergamon, Oxford, England, New York.

Tsuchiya, M., 1986. Thermostads and circulation in the upper layer of the Atlantic Ocean. Prog. Oceanogr. 16, 235–267. https://doi.org/10.1016/0079-6611(86)90040-6.

Tsuchiya, M., 1989. Circulation of the Antarctic Intermediate Water in the North Atlantic Ocean. J. Mar. Res. 47, 747–755. https://elischolar.library.yale.edu/journal_of_marine_research/1949.

Tsuchiya, M., Talley, L.D., McCartney, M.S., 1994. Water-mass distributions in the western South Atlantic; a section from South Georgia Island (54S) northward across the equator. J. Mar. Res. 52, 55–81. https://elischolar.library.yale.edu/journal_of_marine_research/2088.

Vaezzadeh, V., Zhong, G., Zhang, G., 2023. Benzene polycarboxylic acids as molecular markers of black carbon: progresses and challenges. Chemosphere 341, 140112. https://doi.org/10.1016/j.chemosphere.2023.140112.

van der Werf, G.R., Randerson, J.T., Giglio, L., van Leeuwen, T.T., Chen, Y., Rogers, B.M., Mu, M., van Marle, M.J.E., Morton, D.C., Collatz, G.J., Yokelson, R.J., Kasibhatla, P.S., 2017. Global fire emissions estimates during 1997–2016. Earth Syst. Sci. Data 9, 697–720. https://doi.org/10.5194/essd-9-697-2017.

van Heuven, S.M.A.C., Hoppema, M., Huhn, O., Slagter, H.A., de Baar, H.J.W., 2011. Direct observation of increasing CO_2 in the Weddell Gyre along the Prime Meridian during 1973–2008. Deep-Sea Res. II Top. Stud. Oceanogr. 58, 2613–2635. https://doi.org/10.1016/j.dsr2.2011.08.007.

Verwega, M.-T., Somes, C.J., Schartau, M., Tuerena, R.E., Lorrain, A., Oschlies, A., Slawig, T., 2021. Description of a global marine particulate organic carbon-13 isotope data set. Earth Syst. Sci. Data 13, 4861–4880. https://doi.org/10.5194/essd-13-4861-2021.

Virkkula, A., Teinilä, K., Hillamo, R., Kerminen, V.-M., Saarikoski, S., Aurela, M., Viidanoja, J., Paatero, J., Koponen, I.K., Kulmala, M., 2006. Chemical composition of boundary layer aerosol over the Atlantic Ocean and at an Antarctic site. Atmos. Chem. Phys. 6, 3407–3421. https://doi.org/10.5194/acp-6-3407-2006.

Wagner, T., Zabel, M., Dupont, L., Holtvoeth, J., Schubert, C.J., 2003. Terrigenous signals in sediments of the low latitude Atlantic — Implications for environmental variations during the late Quarternary: Part I: Organic carbon. In: Wefer, G., Mulitza, S., Ratmeyer, V. (Eds.), The South Atlantic in the Late Quaternary: Reconstruction of Material Budgets and Current Systems. Springer, Berlin, Heidelberg, pp. 295–322. https://doi.org/10.1007/978-3-642-18917-3_15.

Wagner, S., Brandes, J., Goranov, A.I., Drake, T.W., Spencer, R.G.M., Stubbins, A., 2017a. Online quantification and compound-specific stable isotopic analysis of black carbon in environmental matrices via liquid chromatography-isotope ratio mass spectrometry. Limnol. Oceanogr. Methods 15, 995–1006. https://doi.org/10.1002/lom3.10219.

Wagner, S., Ding, Y., Jaffé, R., 2017b. A new perspective on the apparent solubility of dissolved black carbon. Front. Earth Sci. 5, 75. https://doi.org/10.3389/feart.2017.00075.

Wagner, S., Jaffé, R., Stubbins, A., 2018. Dissolved black carbon in aquatic ecosystems. Limnol. Oceanogr. Lett. 3, 168–185. https://doi.org/10.1002/lol2.10076.

Wagner, S., Brandes, J., Spencer, R.G.M., Ma, K., Rosengard, S.Z., Moura, J.M.S., Stubbins, A., 2019. Isotopic composition of oceanic dissolved black carbon reveals non-riverine source. Nat. Commun. 10, 5064. https://doi.org/10.1038/s41467-019-13111-7.

Wagner, S., Coppola, A.I., Stubbins, A., Dittmar, T., Niggemann, J., Drake, T.W., Seidel, M., Spencer, R.G.M., Bao, H., 2021a. Questions remain about the biolability of dissolved black carbon along the combustion continuum. Nat. Commun. 12, 4281. https://doi.org/10.1038/s41467-021-24477-y.

Wagner, S., Harvey, E., Baetge, N., McNair, H., Arrington, E., Stubbins, A., 2021b. Investigating atmospheric inputs of dissolved black carbon to the Santa Barbara Channel during the Thomas Fire (California, USA). J. Geophys. Res. Biogeosci. 126, e2021JG006442. https://doi.org/10.1029/2021JG006442.

Weiss, R.F., 1970. The solubility of nitrogen, oxygen and argon in water and seawater. Deep-Sea Res. Oceanogr. Abstr. 17, 721–735. https://doi.org/10.1016/0011-7471(70)90037-9.

Weiss, R.F., Östlund, H.G., Craig, H., 1979. Geochemical studies of the Weddell Sea. Deep-Sea Res. A Oceanogr. Res. Pap. 26, 1093–1120. https://doi.org/10.1016/0198-0149(79)90059-1.

Welch, B.L., 1951. On the comparison of several mean values: an alternative approach. Biometrika 38, 330–336. https://doi.org/10.2307/2332579.

Yamashita, Y., Tanoue, E., 2008. Production of bio-refractory fluorescent dissolved organic matter in the ocean interior. Nat. Geosci. 1, 579–582. https://doi.org/10.1038/ngeo279.

Yamashita, Y., Tanoue, E., 2009. Basin scale distribution of chromophoric dissolved organic matter in the Pacific Ocean. Limnol. Oceanogr. 54, 598–609. https://doi.org/10.4319/lo.2009.54.2.0598.

Yamashita, Y., Nakane, M., Mori, Y., Nishioka, J., Ogawa, H., 2022. Fate of dissolved black carbon in the deep Pacific Ocean. Nat. Commun. 13, 307. https://doi.org/10.1038/s41467-022-27954-0.

Yamashita, Y., Mori, Y., Ogawa, H., 2023. Hydrothermal-derived black carbon as a source of recalcitrant dissolved organic carbon in the ocean. Sci. Adv. 9, eade3807. https://doi.org/10.1126/sciadv.ade3807.

Yin, S., Wei, C., Qu, X., Fu, H., Li, B., Piao, S., Tao, S., Hatcher, P.G., Zhu, D., 2024. Benzenepoly(carboxylic acid)s as exclusive intrinsic markers to assess riverine export of dissolved black carbon. Environ. Sci. Technol. 58, 1142–1151. https://doi.org/10.1021/acs.est.3c05988.

Zhang, X., Wang, Y., Liu, Z., Liu, B., Wu, W., Liu, L., He, D., Xu, Y., 2024a. Heterogeneous sources, distribution, and removal processes of dissolved black carbon from East China Sea shelf to open ocean of Northwest Pacific. Prog. Oceanogr. 229, 103374. https://doi.org/10.1016/j.pocean.2024.103374.

Zhang, Q., Zhou, J., Fang, Z., Yang, W., Chen, M., Zheng, M., 2024b. Sources and dynamics of dissolved black carbon in the Pearl River estuary and shelf, northern South China Sea. J. Oceanogr. 80, 71–83. https://doi.org/10.1007/s10872-023-00708-2.

Ziolkowski, L.A., Druffel, E.R.M., 2010. Aged black carbon identified in marine dissolved organic carbon. Geophys. Res. Lett. 37, L16601. https://doi.org/10.1029/2010GL043963.

Ziolkowski, L.A., Chamberlin, A.R., Greaves, J., Druffel, E.R.M., 2011. Quantification of black carbon in marine systems using the benzene polycarboxylic acid method: a mechanistic and yield study. Limnol. Oceanogr. Methods 9, 140–149. https://doi.org/10.4319/lom.2011.9.140.